Volume 49
Number 5
7 March 2020
Pages 1325–1616

Chem Soc Rev

Chemical Society Reviews

rsc.li/chem-soc-rev

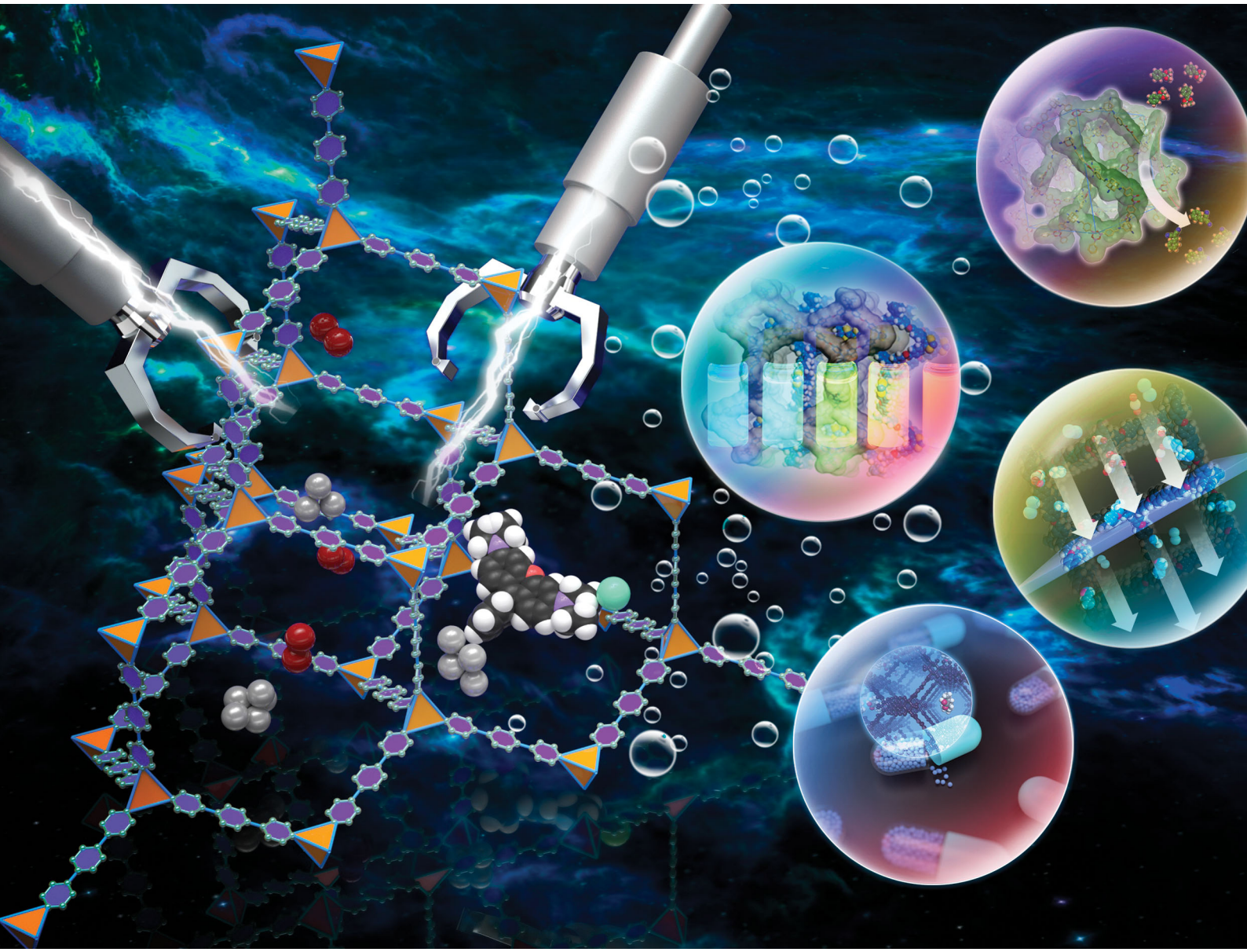

ISSN 0306-0012

ROYAL SOCIETY OF CHEMISTRY

REVIEW ARTICLE

Qianrong Fang, Shilun Qiu *et al.*

Design and applications of three dimensional covalent organic frameworks

Chem Soc Rev

ROYAL SOCIETY OF CHEMISTRY

REVIEW ARTICLE

View Article Online
View Journal | View Issue

Cite this: *Chem. Soc. Rev.*, 2020, **49**, 1357

Design and applications of three dimensional covalent organic frameworks

Xinyu Guan, Fengqian Chen, Qianrong Fang * and Shilun Qiu *

Covalent organic frameworks (COFs), as an emerging class of crystalline porous polymers connected by dynamic covalent bonds, have been well studied over the past decade. Recently, three dimensional (3D) COFs have attracted extensive interest for the synthesis and applications of novel COFs. The principal reason for this rising trend is based on their unique porous features and excellent performances compared to previously reported two dimensional (2D) frameworks with the layered AA-stacking mode. This critical review describes the current state-of-the-art development of 3D COFs in the design principles, synthetic methods, functionalization strategies, and potential applications. Some major challenges associated with future perspectives are further discussed, inspiring the development of 3D COFs.

Received 23rd December 2019

DOI: 10.1039/c9cs00911f

rsc.li/chem-soc-rev

1 Introduction

As a novel class of crystalline porous materials, COFs have attracted wide interest since the pioneering work of Yaghi and co-workers in 2005.[1] Low densities, abundant pore structures and high surface areas are often observed in COFs due to the light element composition and ordered frame structures, making them promising materials in adsorption and separation.[2,3] More importantly, the covalently linked COFs are much more stable than the well-known metal–organic frameworks (MOFs),[4,5] and thus have wider applications as adsorbents in solvents especially in some harsh conditions.[6,7] Furthermore, with a wide choice of monomers and easy modification of pore environments, COFs can provide promising platforms for various applications such as heterogeneous catalysts,[8,9] semiconductors,[10–14] sensors,[15] and others.[16,17]

Based on the different dimensions of the covalently connected frameworks, COFs can be divided into two dimensional (2D) and three dimensional (3D) structures. In 2D COFs, covalent bonds only exist in conjugated 2D sheets while only weak interactions (such as π–π stacking, hydrogen bonds and van der Waals' force) are present in interlayers. In contrast, the whole 3D skeletons are connected by covalent bonds in 3D COFs.

To date, research studies have mainly focused on 2D structures, and reports about 3D COFs are extremely limited. There are still lots of problems that block the exploration of 3D COFs. Firstly, the crystallization problems[18] are more significant for 3D COFs and the synthesis conditions are more rigid and precise for 3D frameworks, especially for those monomers

State Key Laboratory of Inorganic Synthesis and Preparative Chemistry, Jilin University, Changchun 130012, P. R. China. E-mail: qrfang@jlu.edu.cn, sqiu@jlu.edu.cn

Xinyu Guan

Xinyu Guan obtained his BS from Zhejiang University in 2016. Currently, he is finishing his PhD under the supervision of Prof. Qianrong Fang in the State Key Laboratory of Inorganic Synthesis and Preparative Chemistry, Jilin University, China. His current research interests focus on the synthesis and application of covalent organic frameworks.

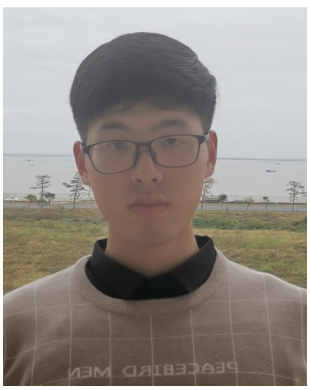

Fengqian Chen

Fengqian Chen received his BS from Yanbian University in 2018. Currently, he is a Master's degree candidate under the supervision of Prof. Qianrong Fang in the State Key Laboratory of Inorganic Synthesis and Preparative Chemistry, Jilin University, China. His current research interests focus on the synthesis and application of covalent organic frameworks.

with functional moieties. Also, 3D COFs are often relatively less stable than 2D structures because of the more empty frameworks and the absence of π–π stacking.[19] Moreover, interpenetrations are common in the 3D network especially in **dia** or **pts** topologies, resulting in highly shrunk channels.[20] Finally, the structural determination is also a bothersome issue, especially for some new topologies or dynamic structures. These problems were discussed in a previous review by Ma and co-workers.[21]

In spite of these problems, 3D COFs are still amazing platforms for further applications due to their unique properties. Generally, there are only uniform one-dimensional channels in 2D COFs while 3D COFs have more complicated pore structures such as interpenetrated channels and cages, which are more beneficial in separation, catalysis, guest incorporation, *etc.* Also, due to the more void frameworks compared to 2D structures, high surface areas, low densities and abundant easily accessible active sites which are highly beneficial for practical usage were often observed in 3D COFs.

A number of reviews have been published for 2D COFs over the past decade, but little discussion about 3D COFs is available. In this review, we firstly introduce the design principle of 3D COFs including topologies, linkages and building blocks. Then the strategy for acquiring functional 3D COFs is presented, followed by applications of these functional materials. Finally, the conclusion and perspectives on 3D functional COFs are proposed.

2 Structural design of 3D COFs

2.1 Topology

Unlike in the case of 2D structures, the topology is a crucially important issue which determines the pore structures, properties and potential applications of 3D frameworks. Since the first 3D COFs reported by Yaghi and co-workers in 2007,[22] there have been only single-digit different topologies in 3D COFs (Fig. 1, **ctn**, **bor**, **dia**, **pts**, **rra**, **srs**, **ffc** and **lon**) and the exploration of novel structures is still the frontier in this field. Crystalline 3D structure preparation and structure determination are still two major challenges for new topology discovery.

Ctn (C_3N_4) or **bor** (boracite) topologies were employed in the earliest 3D COFs, which were formed with tetrahedral plus triangular nodes. By self-condensation reactions of tetrahedral boronic acid or co-condensation with triangular catechol, COF-102, COF-103 and COF-105 were obtained as **ctn** net and COF-108 as **bor** net.[22] The **bor** is about 15% less dense than **ctn** with the same formulas and has larger pores. These frameworks demonstrated 3D-connecting channels and cages, low densities, as well as high surface areas and adsorption capacities.

The following and most universal topology in 3D COFs was the **dia** (diamond) net. The network was constructed by tetrahedral nodes and liner linker. **Dia** is self-dual and prone to self-interpenetration to produce *N*-fold interpenetrated diamond nets (**dia-cN**).[20,23] COF-300 with **dia-c5** was reported as the first 3D COF with **dia** topology.[24] The interpenetration number was determined by complex factors including the distance of two tetrahedral nodes, the steric effect of monomers and the preparation condition of COFs. The first example of 3D COFs with non-interpenetrated **dia** was synthesised with a special building block, 1,3,5,7-tetraaminoadamantane (TAA).[25] A large void space and 3D penetrating channels exist in the non-interpenetrated **dia** skeleton, but only relatively small and one dimensional (1D) channels (*e.g.* 7.2 Å in 5-fold COF-300) remain in highly interpenetrated structures.

In the first one decade of 3D COFs, only three different topologies were reported. In 2016, the fourth topology of 3D COFs, *i.e.*, **pts** (PtS) topology, was reported by Wang and co-workers.[26] The tetrahedral and rectangle building blocks were conjugated to generate such structures. Like the **dia** network, the **pts** net is also likely to form interpenetrated structures. The **Pts** skeleton with a non-interpenetrated structure

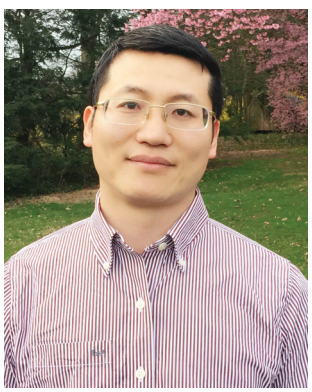

Qianrong Fang

Qianrong Fang received his BS (2001) and PhD (2007) from Jilin University in China. From 2007 to 2014, he completed his postdoctoctoral study in the University of California at Los Angeles, Texas A&M University, University of California at Riverside as well as University of Delaware. In 2015, he received 1000 Young Talent Plan of China and went back to the State Key Laboratory of Inorganic Synthesis & Preparative Chemistry at Jilin University, as a full professor. His current research focuses on the design and synthesis of covalent organic frameworks (COFs) for application in adsorption, separation, catalysis, and other fields.

Shilun Qiu

Shilun Qiu received his PhD in chemistry from Jilin University, China, in 1988. He joined the University de Haute-Alsace for postdoctoral research. In 1994, he was promoted to be a full professor in Jilin University. He won the Second Grade Award for the State Natural Science Award of China in 2008. He received the Guest Professorship in Tohoku University, Drexel University, Stockholm University, and is now the Honorary Professor of University of Queensland. His recent research interests focus on the studies of molecular engineering, synthesis, structure and applications of porous materials and membranes, involving zeolites, mesostructured materials, MOFs and COFs.

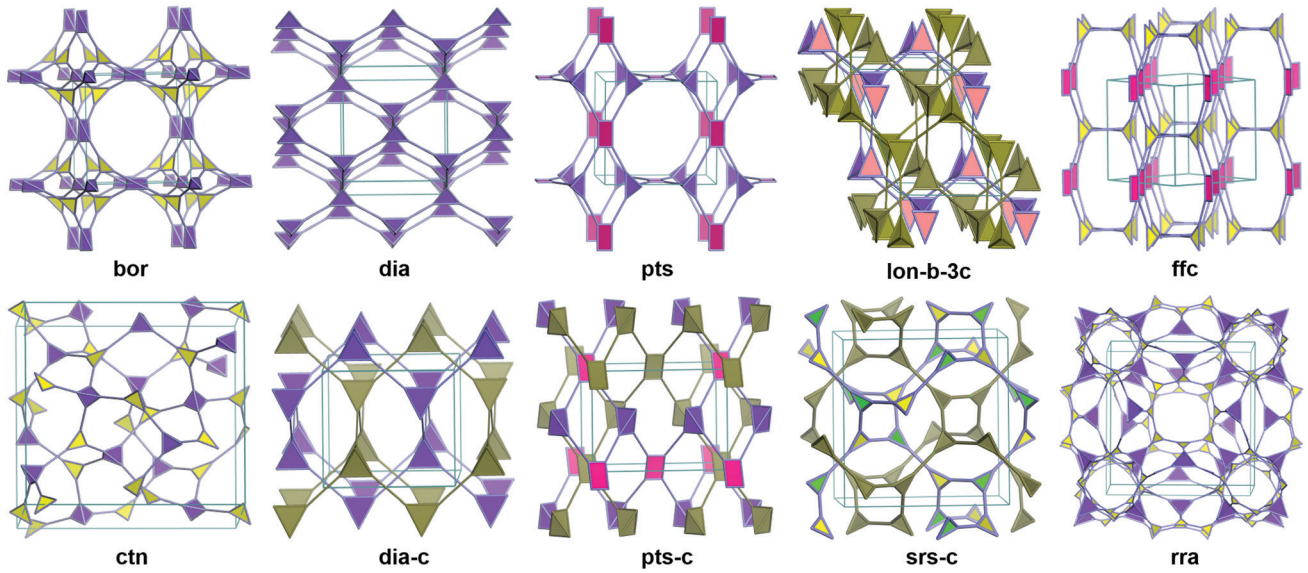

Fig. 1 Topologies in 3D COFs.

(*e.g.* JUC-518[27]) or a small interpenetration number (*e.g.* 3D-Py-COF with two-fold interpenetration) can demonstrate 3D interrelated channels, but only 1D channels persist in those with high interpenetration (*e.g.* 3D-TPE-COF with the seven-fold interpenetrated **pts** net[28]).

All the topologies mentioned above were based on at least one tetrahedral monomer, which significantly limits the structural diversity of 3D COFs. The exploration of new topologies was essential for 3D COFs.

In 2017, Feng and co-workers proposed brand new CD-COFs based on **rra** topology.[29] CD-COFs were produced by covalently joining γ-cyclodextrin (γ-CD) molecules *via* spiroborate linkages. In this structure, each boron atom is joined to four γ-CD struts, and each γ-CD is connected to eight boron atoms. The tetrakis(spiroborate) linkages and glucopyranose species were regarded as tetrahedral and triangular nodes respectively to give **rra** topology with 3D interconnected channels.

Another topology such as **srs** (SrSi) was reported in 2018 by Thomas and co-workers.[30] Hexahydroxytriphenylene moieties were conjugated with dianionic hexacoordinate $[SiO_6]^{2-}$ linkages. It is notable that the hexacoordinate $[SiO_6]^{2-}$ were octahedral and three catechols that were coordinated to the same Si were not coplanar, and thus the frameworks of these SiCOFs were obtained as a 3D network with new **srs** topology.

Also in 2018, Yang and co-workers synthesized a series of COFs with the new **ffc** topology.[31] This was the first example of 3D COFs without the employment of 3D monomers or linkages. The new topology was generated with tetragonal and triangular monomers and 3D penetrated channels existed in the frameworks.

A rare **lon** (lonsdaleite) topology was discovered by Wang and co-workers in 2018. **Lon** topology was composed of two different tetrahedral building blocks. A three-fold interpenetrated **lon** network related by a threefold axis (**lon-b-c3**) was reported in the paper, being a rare example of class IIa of interpenetration. The **lon-b-c3** framework was chiral, originating from the three-fold interpenetration and the intersection of the network generated a 6_5 screw axis.

To provide guidance for new topologies, some efficient predictive modeling methods were introduced, and some possible topologies (**tfj**, **fjh**, **iab**, **sod**, **cda**, **cds**, **pcu**, **acs**, **bcu** and **ttt**) were also proposed.[31,32]

2.2 Linkage

Linkages in 3D COFs were rigid and dynamic, which was the basic principle of COF linkages.[33,34] Most of the linkages of 3D COFs have been employed in 2D structures previously, but only a few dynamic reactions used in 2D COFs were transferred into 3D COFs successfully, possibly on account of the difficulties in 3D COF preparation and characterization. The introduction of linkages from 2D COFs (such as triazine,[35] azine,[15] hydrazone,[36] urea,[37] alkene,[38] and so on) is still an interesting topic in developing new 3D COFs. We have summarized the reactions and linkages used in 3D COFs in Fig. 2. During the first few years of 3D COFs, the linkages were mainly generated with boronic acid. In the first report by Yaghi and co-workers, two different linkages were proposed.[22] Boroxine rings were generated from the trimerization of boronic acids in COF-102 and COF-103, and boronate ester rings were produced through the co-condensation of boronic acids and catechols in COF-105 and COF-108. Both reactions were highly reversible and rigid rings were generated as linkages. High crystalline and high surface areas can be observed in this kind of structures, but the insufficient chemical stability became a bottleneck for further development of these materials. As a result, 3D COFs linked by boroxine rings or boronate esters were hot topics only in the early periods and no application was explored with this kind of materials other than gas storage.

After that, the imine bond, the most widely studied linkage in COFs,[39] was put forward by Yaghi and co-workers in 2009.[24]

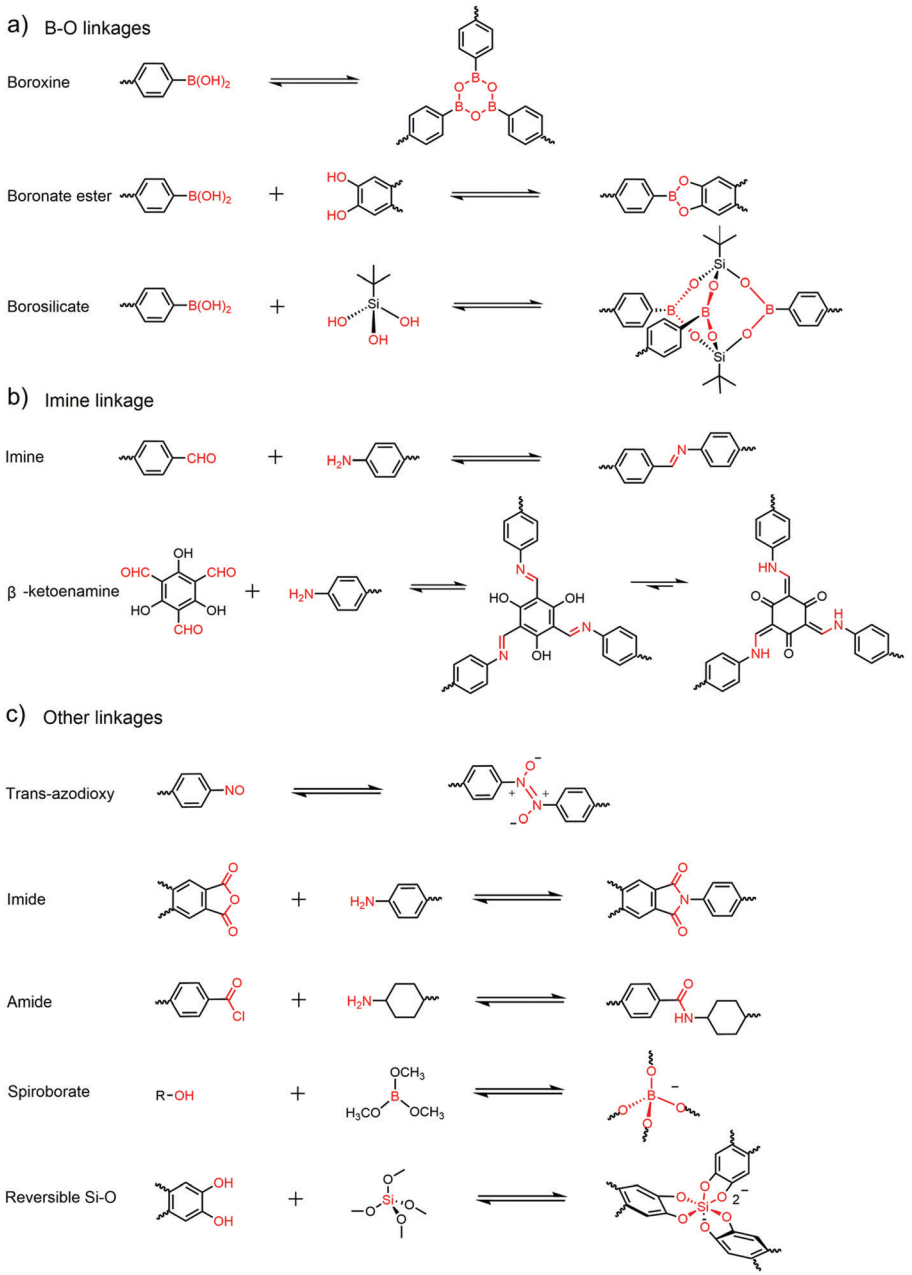

Fig. 2 Linkages in 3D COFs.

The imine bond was generated through reversible dehydration reaction between primary amine and aldehyde with acid catalysts (mostly acetic acid). Compared to previous structures which even cannot tolerate water or moisture, significantly enhanced chemical stability was observed in imine-linked COFs. With the employment of the tri-link monomer triformylphloroglucinol (TFP), the β-ketoenamine linkage which exhibited ultrahigh chemical stability in 2D frameworks was incorporated in 3D COFs for the first time by Fang and co-workers.[40] Owing to the high crystallinity, adequate chemical stability and easily designable structures, imine-based COFs have dominated the research on 3D COFs since being created. However, the chemical stability of some 3D imine COFs, especially in some empty frameworks, is still not adequate enough, so the development of novel linkages in 3D COFs was still waiting for further exploration.

Other than the two major classes of linkage, some other linkages have also been generated in 3D COFs. Nonetheless, studies of these linkages are limited and only one paper was reported for each linkage in 3D COFs.

The borosilicate cluster was another linkage based on boronic acid reported in 2008.[41] The rigid borosilicate cages which were obtained by condensation of *tert*-butylsilane triol with boronic acid functioned as three-coordinated vertices in COF-202. Unfortunately, no other work has been reported on this linkage.

In 2013, Wuest and co-workers reported a series of 3D COFs (NPN-1, NPN-2, and NPN-3) based on *trans*-azodioxide linkages,

which were formed by dimerization of nitrosos.[42] These materials were readily available as the rare single crystal morphology in COFs and some interesting properties like molecular weight and dispersity were studied for the first time. Unfortunately, no stability test was conducted in this work and no additional work was reported for these materials.

Imides or amides have also been utilized in 3D COFs. In 2015, two 3D polyimide COFs (PI-COF-4 and PI-COF-5) were manufactured by Fang and co-workers.[25] These frameworks were connected by imides through imidization of primary amines and dianhydride. 3D PI-COFs demonstrated high stability and were employed in controlled drug delivery. CAF-2[43] with amide linkage was prepared with tetra-functional 4,4′,4″,4‴-methanetetrayltetrabenzoic chloride (MTABC) and di-functional *trans*-1,4-cyclohexanediamine (CHDA) in 2017. Due to the high stability of amide bonds, CAF-2 can survive in water, 1 M HCl or 1 M NaOH for 24 h at 100 °C or in 12 M HCl or 14 M NaOH for 1 week at room temperature. However, the preparation of CAF-2 was kind of complicated and required a transformation from the amorphous network.

And lately a couple of anionic polyhedra were designed as the connecter of 3D COFs. In 2017, CD COFs[29] with anionic tetrakis(spiroborate) $[BO_4]^-$ were generated through the thermodynamically controlled transesterification reaction between hydroxy groups and trimethyl borate ($B(OMe)_3$). Unlike linear or planar linkages mentioned above, tetrakis(spiroborate) came as the first tetrahedral linkage formed in 3D COFs. Various counterions can be used in the structures, significantly broadening the structural diversity and potential applications of this kind of material.

Another type of anionic COFs, 3D silicate COFs (SiCOFs), was reported by Thomas and co-workers in 2018.[30] The novel $[SiO_6]^{2-}$ linkage was produced by reversible Si–O formation between catechols and MTMS. However, no application research was conducted over these materials, possibly due to the relatively low chemical stability of the $[SiO_6]^{2-}$ linkage.

It is worth noting that borosilicate cages, *trans*-azodioxide and anionic $[BO_4]^-$ and $[SiO_6]^{2-}$ were the unique linkages in 3D COFs which have never been presented in 2D COFs.

2.3 Building blocks

Other than the rare examples of **rra**, **srs** and **ffc** topologies, most 3D COFs are prepared with tetrahedral building blocks, which are generally composed of a tetrahedral core and four identical functional groups (Fig. 3). Only a few tetrahedral monomers are available in 3D COFs and most possible combinations of cores and functional moieties are lacking.

Most of the tetrahedral cores adopt T_d symmetry if not taking into account phenyls. Tetraphenylmethane (TPM) is the most common knot with various functional groups, including boronic acid,[22] amino,[24] aldehyde,[44] nitrosos,[42] acyl chloride[43] and salicylaldehyde.[45] Tetraphenylsilane (TPS) with boronic acid,[22] aldehyde[46] or nitrosos[42] as well as 1,3,5,7-tetraphenyladamantine (TPA) with amino[47] or nitrosos[42] has also been used in 3D COFs. Recently, tetrahedral nodes with longer arms were also developed but only salicylaldehyde derivatives were available such as tetra(1,1′-biphenyl-4-yl)methane (TbPM) and tetra(1,1′-biphenyl-4-yl)silane (TbPS).[48] TAA[40] with an adamantane core was the only aliphatic tetrahedral monomer without phenyls. Interestingly, the interpenetration number can be significantly

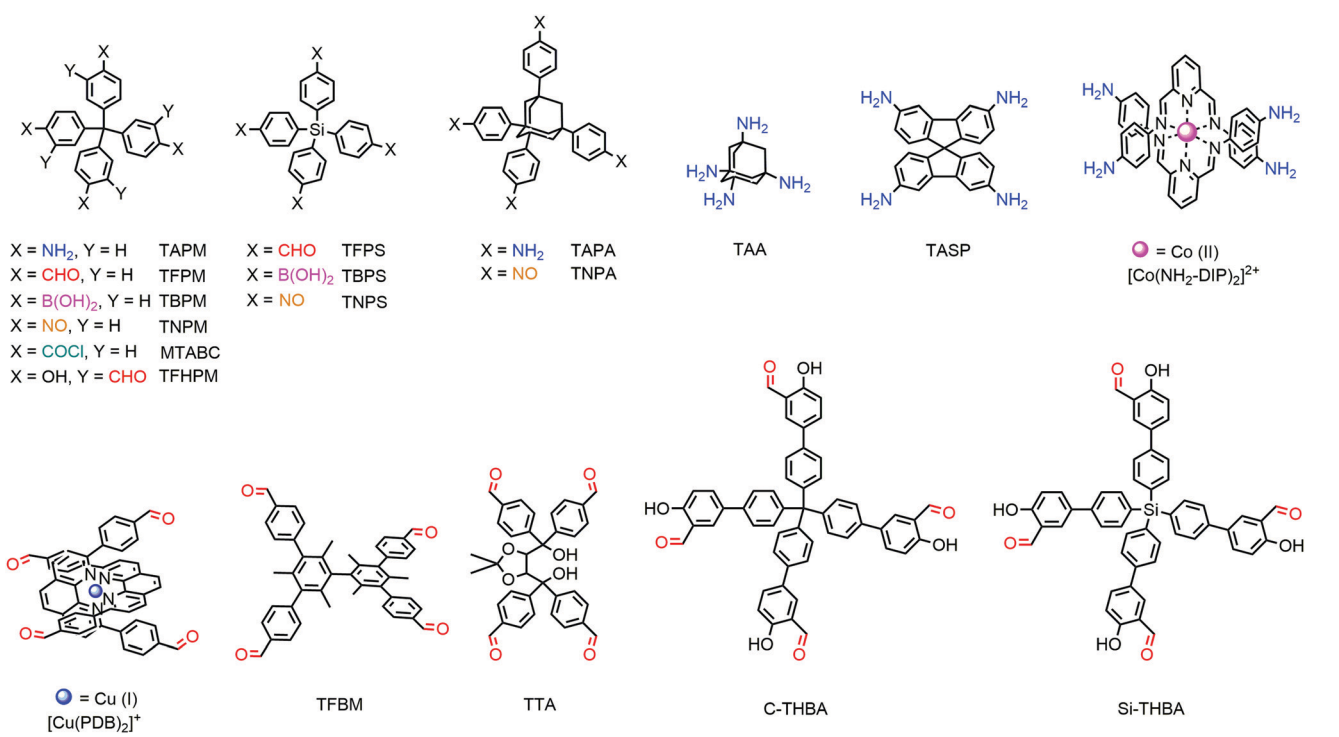

Fig. 3 Tetrahedral building blocks in 3D COFs.

decreased with the employment of TAA. Recently, some tetrahedral cores with lower symmetry have also been employed, such as the conjugated spirobifluorene (SP)[49] or chiral tetraaryl-1,3-dioxolane-4,5-dimethanol (TADDOL)[50] backbone.

Steric hindrance might be a new approach for tetrahedral building blocks. For example, free biphenyl was inclined to form planar conformation in 2D COFs with the assistance of strong π–π stacking, but 3,3′,5,5′-tetrakis(4-formylphenyl)-bimesityl (TFBM) with six methyl groups that limited the rotation of biphenyl can serve as a tetrahedral building block in 3D COFs.

Another interesting set of tetrahedral synthons was raised by Yaghi and co-workers in woven COFs,[51,52] which was based on tetrahedral metal chelate compounds. $[Cu(PDB)_2]^+$ with four aldehyde groups of tetrahedral geometry was the first proposed synthon of woven COFs. It should be noted that the two PDB moieties were not covalently connected and the orientation of the PDB units was confined by the cuprous ion. Bis(diiminopyridine) complexes $[Co(DIP)_2]^{2+}$ in which the four amino groups were tetrahedral were also used as the nodes in woven COFs.[53]

Other than tetrahedral building blocks, γ-CD[29] was the only steric monomer (Fig. 4). Some planar synthons are also summarized in Fig. 4.

2.4 Synthetic methods and morphology

2.4.1 Polycrystal. Most of the COFs were prepared as polycrystalline powders and the most widely used approach was the solvothermal approach. To address the problems faced in solvothermal synthesis, some new methods were introduced, including microwave synthesis, ionothermal synthesis, devitrification and linker exchange.

Since first proposed by Yaghi and co-workers in 2007, the solvothermal approach has been the most prevalent method for 3D COF preparation and most of the 3D COFs can be acquired through this way. The typical procedures were carried out by suspending monomers in a mixture of solvents and catalysts followed by heating at 120–160 °C for 3–7 days in sealed tubes or autoclaves. However, a great deal of trials was necessary before getting the suitable conditions for preparation. A number of variables had to be adjusted including the composition of solvents, concentration of catalysts, temperature of the reactions, *etc.* Moreover, high-temperature and high-pressure conditions, complicated operations, and long reaction periods were the drawbacks faced by solvothermal synthesis. In the past few years, it became more and more important for scientific researchers to develop simple and green methods for the preparation of 3D COFs.

Microwave synthesis is well-known for small molecule synthesis due to accelerated reaction times, cleaner products, and higher yields in many cases. In 2009, Cooper and co-workers reported the microwave synthesis of COF-102.[54] The reaction was completed within 20 min, being more than 200 times faster than the reported solvothermal reaction time of 72 h. PXRD, FTIR and N_2 adsorption isotherm of the acquired material were broadly comparable to those prepared by solvothermal processing. CD COFs were also prepared under microwave-assisted solvothermal conditions in 2017.

For those COFs with strong bonds, devitrification might be a meaningful approach. Covalent amide frameworks (CAFs) could not be obtained through the direct solvothermal approach due to the low reversibility of amide bonds. But in 2017, CAF-2 was successfully acquired by subjecting the amorphous polyamide network (PATCnC) to the devitrification method (at 240 °C for 7 days with 15 molar equivalents of water, cooling at 0.1 °C min^{-1}).[43]

Ionic liquids (ILs) have recently drawn broad attention as green and safe reaction media due to their peculiar properties including negligible vapor pressure, non-flammability, wide liquid range, good solubility in both organic and inorganic compounds and highly designable structure. In 2018, Fang and co-workers proposed the brand new fast ionothermal synthesis for preparing a series of 3D-IL-COFs.[55] The syntheses were carried out under ambient temperature and pressure and can be completed in a short period (*e.g.*, only three mins for 3D-IL-COF-1). 1-Butyl-3-methylimidazolium bis((trifluoromethyl)sulfonyl)imide ([BMIm][NTf_2]) was the typical ionic liquid used in this work and other ILs like 1-butyl-3-methylimidazolium dicyanamide ([BMIm][$N(CN)_2$]) were also practicable. Ionic liquids played the role of both solvents and catalysts and can be simply recycled at least three times without significant activity loss.

Recently, the linker exchange approach which was previously used in 2D COFs[56] has also been reported for 3D COFs. Both COF-320-to-COF-300 and the opposite COF-300-to-COF-320 transformations were successfully achieved.[57] Meanwhile, a new network containing two dialdehyde monomers was produced during the COF-300 to COF-320 transformation procedure, which can be verified indirectly by studying the structure of COF-300–320.

Although various pathways have been developed for 3D COFs, new methods were still under exploration for 3D COF preparation. It might be inspirational to borrow some strategies from other porous organic polymers,[58] especially 2D COFs, such as mechanochemical synthesis,[59] flow synthesis[60] or vapour-assisted conversion.[61]

2.4.2 Single-crystal. The structural determination of polycrystalline 3D COFs was difficult especially when they are not based on the anticipated frameworks. Moreover, atomic positions and geometric parameters and guest arrangements were often not available in coarse crystal structures acquired from powder X-ray diffraction (PXRD). The growth of single crystals might be the perfect key to all the problems but the realization was difficult. It is still a hot issue to develop a universal and efficient approach for preparing single crystalline COFs.

The first report for 3D COFs that can be fully characterized by single-crystal X-ray diffraction (SXRD) came out in 2013.[42] NPN-1, NPN-2 and NPN-3 with *trans* azodioxide linkages were prepared by crystallization from the solution of tetra-functional nitroso. The crystals more than 10 μm (up to 0.5 mm for NPN-3) were obtained and subjected to SXRD. This was a very successful example but was successful only with the rare azodioxide linkages.

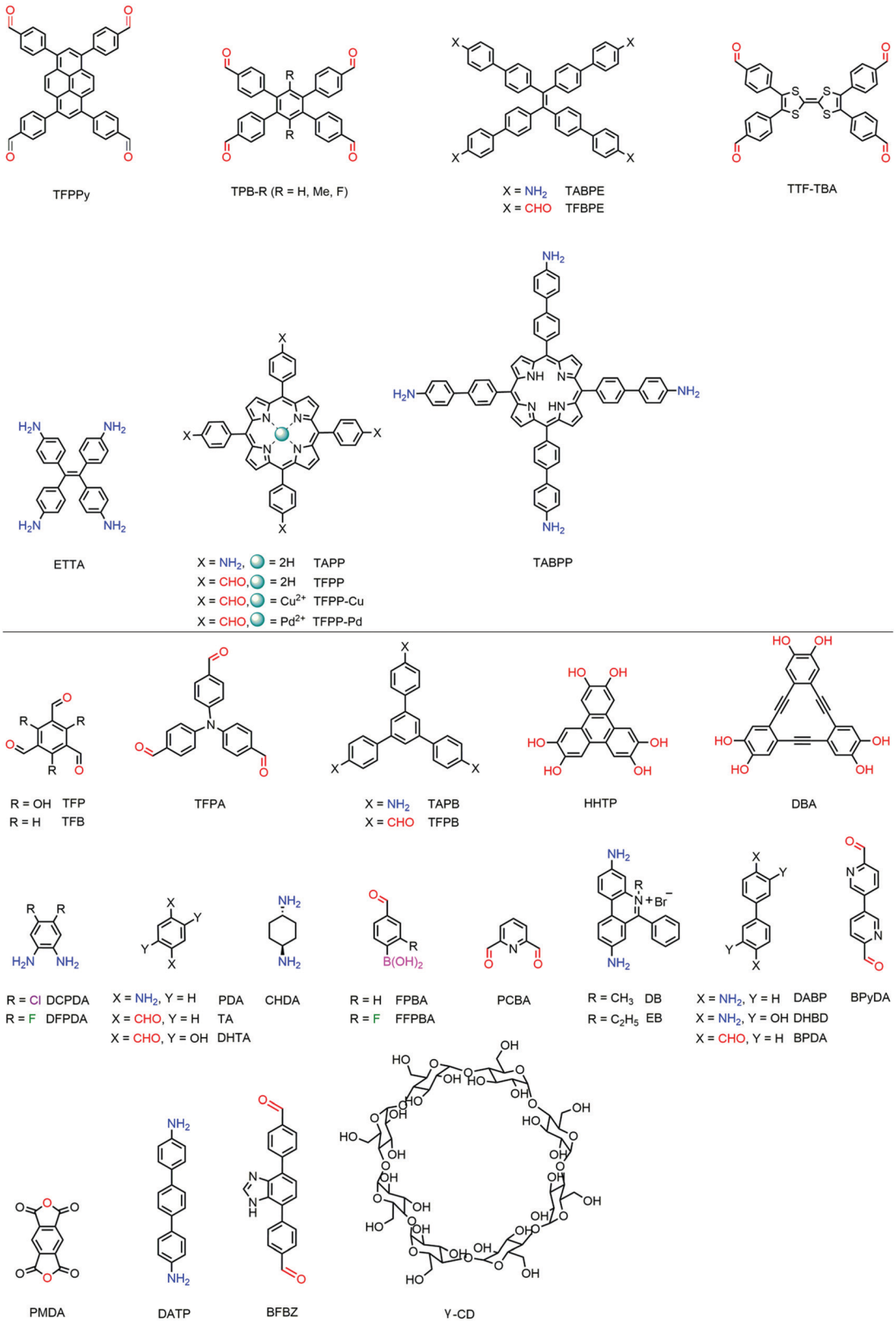

Fig. 4 Various building blocks in 3D COFs.

In the same year, Yaghi and co-workers also reported single crystals for imine-linked COF-320 prepared by the traditional solvothermal approach.[62] However, the crystals in this paper were too small ($1.0 \times 0.5 \times 0.2\ \mu m^3$) for SXRD and only single-crystal 3D

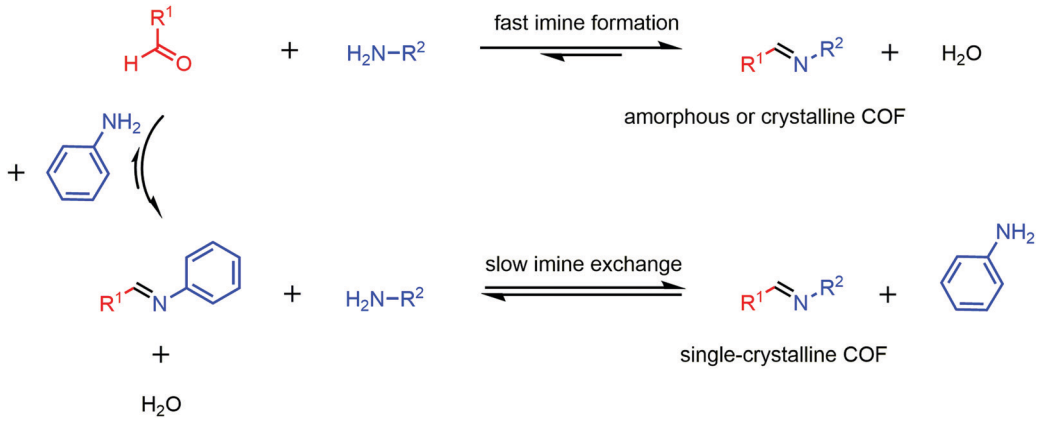

Fig. 5 Growth of 3D imine COF single crystals modulated by aniline.

electron diffraction using the rotation electron diffraction (RED) method was used for structure resolution.

The new strategy proposed by Wang and co-workers in 2018 for growing large single crystalline COFs marked a technical milestone in this area (Fig. 5).[46] The monofunctional aniline was used as a modulator to alter the crystallization process. Four 3D imine COFs (COF-300, COF-303, LZU-79 and LZU-111) were prepared as single crystals up to 100 μm and the structures were defined by SXRD. However, a long time (*e.g.* 30–40 days for COF-300 with the average size of 60 μm) was required for single crystal growth in this work and no further work was reported based on this approach.

Interestingly, most of single crystals reported for COFs were 3D structures, possibly because of higher reversibility in 3D COF formation. The only single-crystal 2D COFs were prepared through seeded growth,[63] which might be another possible approach for single-crystal 3D COFs.

2.4.3 Membrane. Due to the abundant open channels, high surface areas and promising stability, it is highly attractive to develop 3D COF membranes for potential application in gas separation, storage, catalysis, optoelectronics, *etc.* Several strategies have been developed for preparing 2D COF thin films, including bottom-up growth and top-down exfoliation.[64] Top-down approaches were significantly unsuitable for 3D COFs since the whole frameworks were connected by strong covalent bonds and no separated domains existed. Bottom-up methods for 2D COFs include solvothermal synthesis, flow synthesis,[65] vapour-assisted conversion[66] or interfacial synthesis,[67,68] but it was also troublesome to control the thickness of 3D COF films since anisotropism was not so obvious in 3D COFs as in 2D. To date, only a handful of works have been reported for 3D COF membranes.

The first 3D COF membrane was fabricated on porous ceramic α-Al_2O_3 substrates (Fig. 6a).[69] The substrate was first

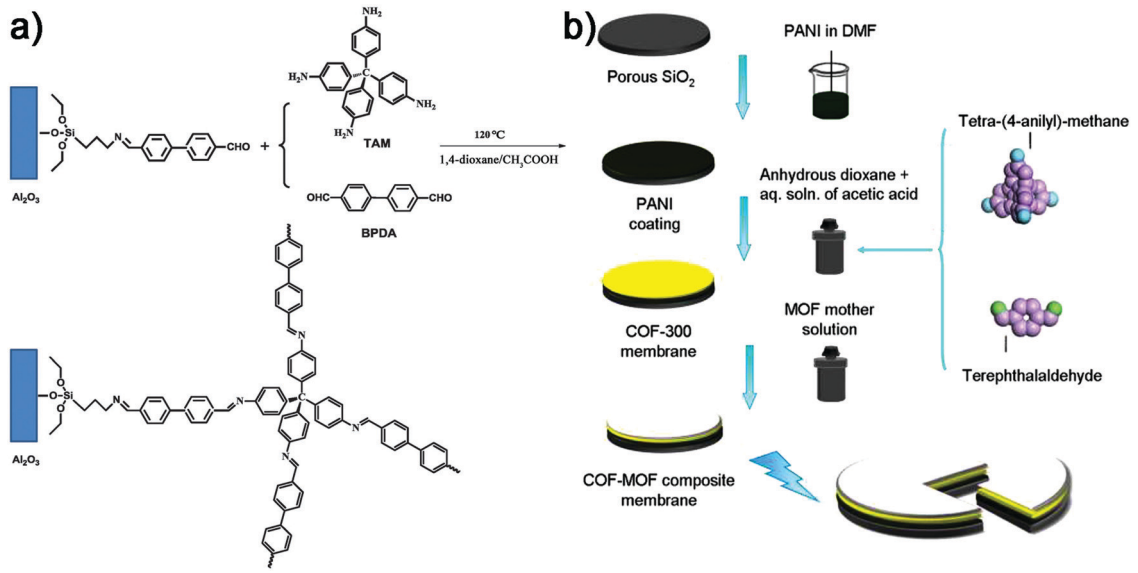

Fig. 6 (a) Fabrication of the COF-320 membrane on modified porous Al_2O_3 (reproduced from ref. 69 with permission from Royal Society of Chemistry, Copyright 2015). (b) Fabrication of the COF-300 membrane and further COF–MOF composite membranes on modified porous SiO_2 (reproduced from ref. 70 with permission from American Chemical Society, Copyright 2016).

modified with 3-aminopropyltriethoxysilane (APTES) and the terminal amino groups of APTES were reacted with BPDA followed by the formation of a 3D COF-320 membrane in the presence of tetrakis(4-aminophenyl)methane (TAPM) and biphenyl-4,4′-dicarbaldehyde (BPDA) under solvothermal conditions. Scanning electron microscope (SEM) images indicated that the COF-320 membrane was homogeneous and compact and the thickness was about 4 μm. This strategy can significantly extend the choice of various substrates, including crystal facets such as Au(111) and Ag(111), or single-layered graphite/highly ordered pyrolytic graphite (SLG/HOPG). In another work, the porous SiO_2 disk was first modified by polyaniline (PANI) followed by heating in COF-300 mother solution (36.00 mg terephthalaldehyde (TA) and 60.00 mg TAPM, 3.00 mL anhydrous 1,4-dioxane (3.00 mL) and 0.60 mL of 3.00 M aqueous solution of acetic acid) to obtain the COF-300 membrane (Fig. 6b).[70] Similar procedures were used for further preparation of COF–MOF composite membranes.

The formation of mixed matrix membranes (MMMs) was another approach for preparing COF based separation membranes. In the following work by Khan and co-workers (Fig. 7),[71] COF-300 prepared previously through the traditional solvothermal method was functionalized with poly(ethyleneimine) (PEI), dispersed in solutions and added dropwise into the polymer solution (glassy 6FDA-DAM or rubbery Pebax) to get a 6 wt% membrane casting suspension. Then the suspension was transferred onto a flat glass Petri dish by a conventional solution casting method to get the MMM membrane with COF fillers.

3 Functional incorporation in 3D COFs

The functions and properties of 3D COFs often come from the pore structure and functional groups. Generally, functional moieties can be introduced into the materials through the modification of COF precursors (bottom-up approach), *via* the incorporation after COF formation (post modification) or in parallel with the formation of the framework (*in situ* approach).

3.1 *In situ* approach

Some linkages generated during COF formation demonstrated excellent performance for various applications such as gas adsorption and catalysis, and these functionalization strategies were regarded as *in situ* approaches. This is an easy approach but the functional moieties are limited.

BF-COFs[40] were the first examples for the practical applications of this kind of functional COFs. Two 3D imine COFs (BF-COF-1 and BF-COF-2) were synthesized based on TAA. The Schiff base groups in the frameworks were found to be alkaline (Fig. 8a) and both COFs were used as promising base catalysts. A similar strategy was used for acid–base bifunctional DL-COFs.[72] With the design of monomers, both acidic boroxine groups and basic imine sites were generated in the same network (Fig. 8b) and showed excellent bifunctional catalytic activities for one-pot cascade reactions.

Salphen and salen moieties can also be brought into 3D COFs through this strategy (Fig. 8c). In 2019, JUC-508 and JUC-509 were generated with a tetrahedral salicylaldehyde-based monomer and amine-based linkers.[45] The easily accessible salphen groups were produced and their metal derivatives were used as catalytic

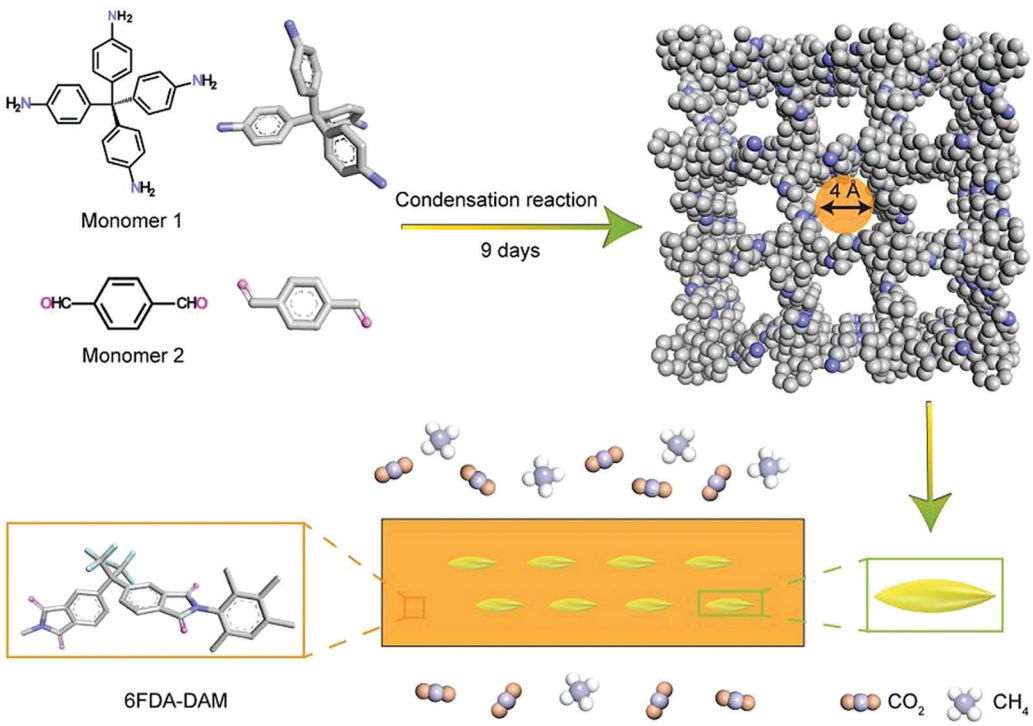

Fig. 7 Preparation of the COF-300 based MMM membrane (reproduced from ref. 71 with permission from Royal Society of Chemistry, Copyright 2019).

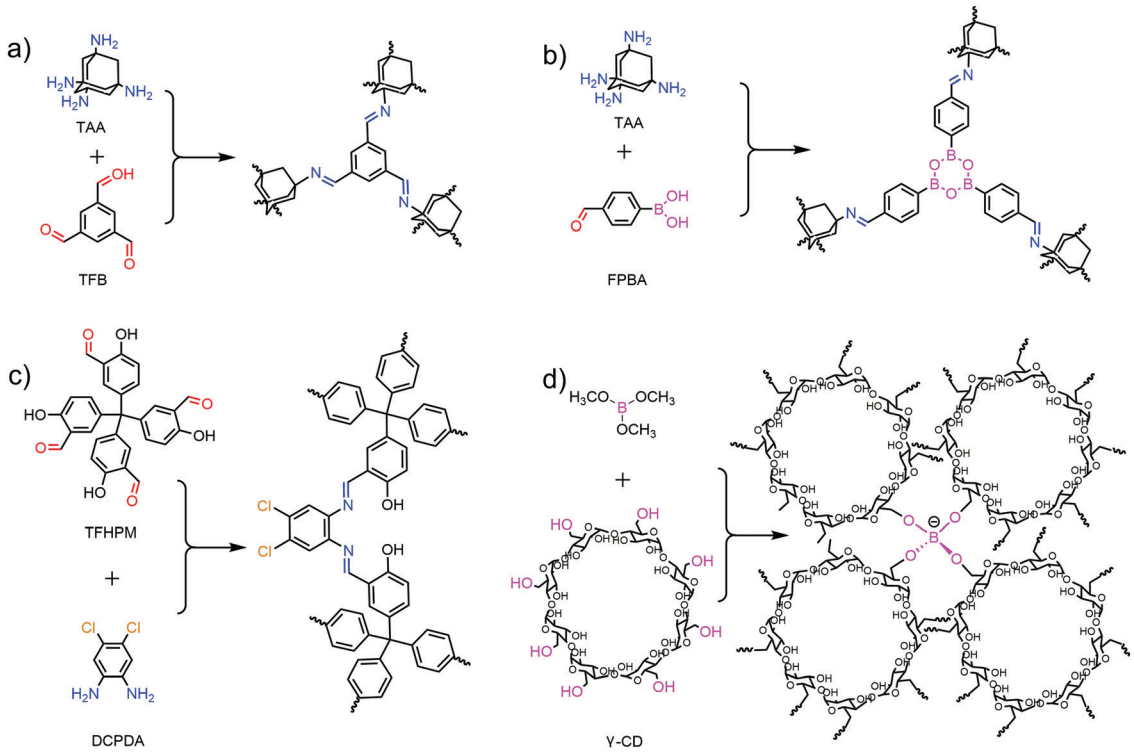

Fig. 8 (a) Base sites generated in BF-COFs. (b) Acid and base sites generated in DL-COFs. (c) Salphen groups generated in JUC-508 and JUC-509. (d) Anionic tetrakis(spiroborate) moieties generated in CD-COFs.

antioxidants. Later in the same year, COF 1 and COF 2 with salen groups were reported in an individual work.[48] Two different tetrahedral salicylaldehyde-based monomers were selected and coupled with ethanediamine to produce salen moieties together with the framework.

The introduction of anionic centres has also been reported. In 2017, 3D CD-COFs with anionic tetrakis(spiroborate) linkages were constructed from hydroxyl-containing γ-CD and trimethyl borate (Fig. 8d). The ordered channels and anionic skeleton made this material a potential candidate for Li ion conduction.

3.2 Bottom-up approach

In this method, the functional groups were anchored onto monomers before COF synthesis. The structural breaking which often occurs in the post-functionalization method can be avoided and the quantity of active sites can be controlled accurately. Nevertheless, the crystallization procedure is more difficult with the pre-functionalized monomers especially those with large moieties or reactive sites. To date, various functional groups important in organic chemistry have been introduced into 3D COFs.

In the early years, the modifications of 3D COFs were mainly based on the truncated mixed-linker (TML) approach. In the paper of Dichtel and co-workers in 2012, COF-102-C_{12} and COF-102-allyl were obtained by condensing mixtures of tetrahedral TBPM with truncated monomers (one of the arylboronic acids in tetra(4-dihydroxyborylphenyl)methane was replaced by a relevant functional group) (Fig. 9a).[73] The degree of functionalization was determined by the feed ratio of the two monomers and loadings of the truncated monomer can reach up to 30%. Two years later, and also by Dichtel and co-workers, COF-102-tolyl was obtained by truncating COF-102 with the monofunctional comonomer *p*-tolylboronic acid (Fig. 9b).[74] Incorporation values (TTolyl) can reach up to 33%. COF-102 with other functionalizations like COF-102-nonyl, COF-102-vinyl, and COF-102-formyl were also successfully obtained by changing different monofunctional compounds.

Different from the TML approach, the preparation for imine-based 3D functional COFs was mainly based on a predesigned functional amine/aldehyde monomer and a traditional tetrahedral aldehyde/amine monomer.

Fluorophores were first introduced into 3D COFs through this way. In 2016, 3D-Py-COF, a pyrene based 3D COF, was prepared with the monomer 1,3,6,8-tetrakis(4-formylphenyl)-pyrene (TFPPy) and exhibited intense yellow-green luminescence.[26] Later, tetraphenylethylene (TPE), the representative aggregation-induced emission (AIE) luminogen, was also brought into 3D-TPE-COF with monomer 1,1,2,2-tetrakis(4-formyl-(1,1′-biphenyl))-ethane (TFBPE).[28]

Most of the COFs were neutral and the ionic 3D COFs were also constructed by the bottom-up strategy. Fang and co-workers reported two 3D-ionic-COFs which were obtained through the polymerization of TFPM with the ionic synthons diimidium bromide (DB) or ethidium bromide (EB).[44] The anionic sites were easy to access in the channels and ion exchange can take place in 3D-ionic-COFs.

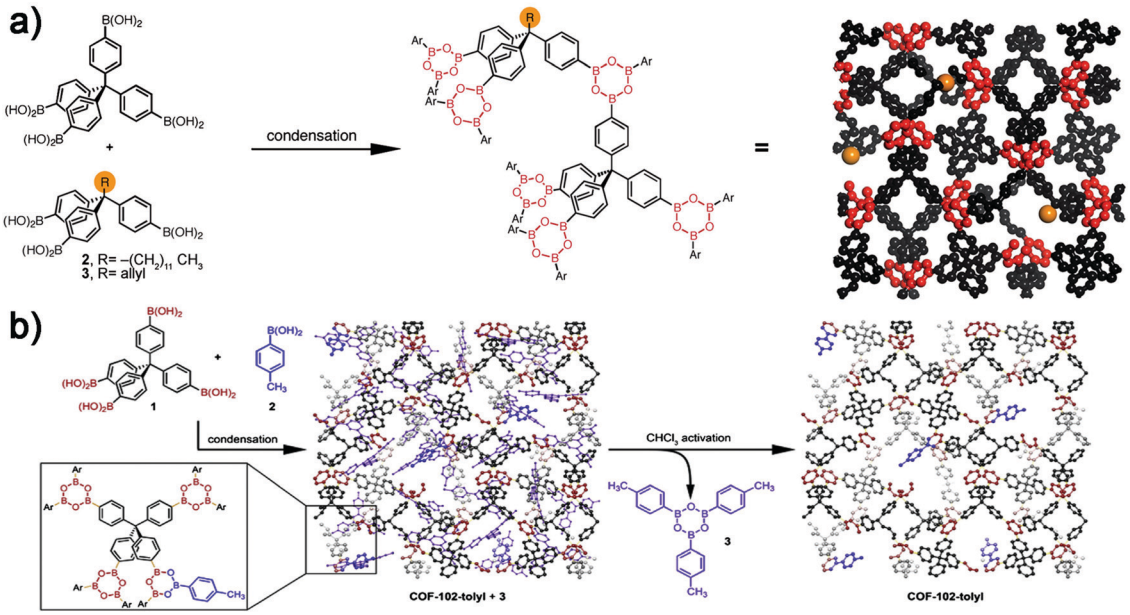

Fig. 9 (a) TML approach in the synthesis of COF-102-C12 and COF-102-allyl (reproduced from ref. 73 with permission from Wiley-VCH, Copyright 2012). (b) Synthesis of COF-102-tolyl (reproduced from ref. 74 with permission from Royal Society of Chemistry, Copyright 2014).

As an important part in metal–organic chemistry, porphyrin and metallized porphyrin have also been incorporated into 3D COFs. The synthesis of 3D porphyrinic COFs (3D-Por-COF and its metal derivatives) mainly relies on the planar quadridentate 5,10,15,20-tetrakis(4-formylphenyl)porphyrin (TFPP) and its derivatives. 3D-Por-COF and 3D-CuPor-COF[75] were first reported by Wang and co-workers in 2017 followed by 3D-PdPor-COF[76] reported by the same group in 2019. These frameworks possessed exposed porphyrin sites and were potential in adsorption and catalysis.

The only literature of chiral 3D COFs was also based on this pathway. The first chiral 3D COF (CCOF 5) was reported by Liu and co-workers in 2018.[50] The key point of this procedure was based on a brand new chiral tetrahedral enantiopure teraaldehyde TTA. The chiral tubular channels in the framework suggested it to be a promising material for enantiomer separation.

Recently, tetrathiafulvalene (TTF), an important redox and electrochemical active group, was also used in 3D COFs by Fang and co-workers.[27] The plane monomer used in this work was tetrathiafulvalene-tetrabenzaldehyde (TTF-TBA) and two different tetrahedral amines (TAA and TAPM) were employed.

3.3 Post-synthetic approach

The post-synthetic approach is widely used in the preparation of functional 3D COFs. The pristine networks without functionality are prepared and then the functional moieties are anchored to obtain target functional 3D COFs. As the structure and porosity may be damaged under some treatments during post-modification, the development of mild modification methods was a hot topic in the last decade. Compared to the bottom-up approach, the quantities and distributions of active sites were difficult to control after post-modification.

In fact, since the post-synthetic approach often needed initial binding sites on the pristine scaffold, this method was commonly used in combination with the bottom-up approach or the *in situ* approach. Generally, the pre-designed monomers with a small steric effect and little reactivity were adopted in pristine COF preparation, and the obtained parent frameworks were further modified under mild conditions.

The pioneering work came in 2013 by Dichtel and co-workers.[77] The thioether-modified COF-102-SPr was produced by subjecting pre-designed COF-102-allyl to typical thiol–ene reaction conditions (Fig. 10a). ^{1}H nuclear magnetic resonance (NMR) analysis of hydrolyzed COF-102-SPr indicated the complete disappearance of allyl groups and the high efficiency of the thiol–ene reaction within the pores of COF-102-allyl.

Other than the thiol–ene click reaction, the ring opening reaction was also employed for 3D COF modification. In 2018, Fang and co-workers reported the preparation of 3D-COOH-COF by conducting the ring opening reaction of succinic anhydride (SA) over hydroxyl-functionalized 3D-OH-COF (Fig. 10b).[78] High crystallinity and porosity were retained after modification. Elemental analysis and liquid 1H NMR spectroscopy of the hydrolyzed sample confirmed that 50% of hydroxyls were grafted with carboxylic groups.

Both the works above needed a predesigned pristine framework with reactive functional groups. However, linkages formed in 3D COFs can also serve as the modified sites. In 2018, Deng and co-workers carried out the transformation from imine linked COF-300 to amine linked COF-300-AR by direct reduction (Fig. 11a), which was confirmed by PXRD and Fourier transform infrared spectroscopy (FTIR).[79] Interestingly, the direct synthesis of amine-linked COFs through the traditional solvothermal approach has not been reported.

Another example of linkage transformation in 3D COFs was reported by Liu and co-workers at almost the same time.[50]

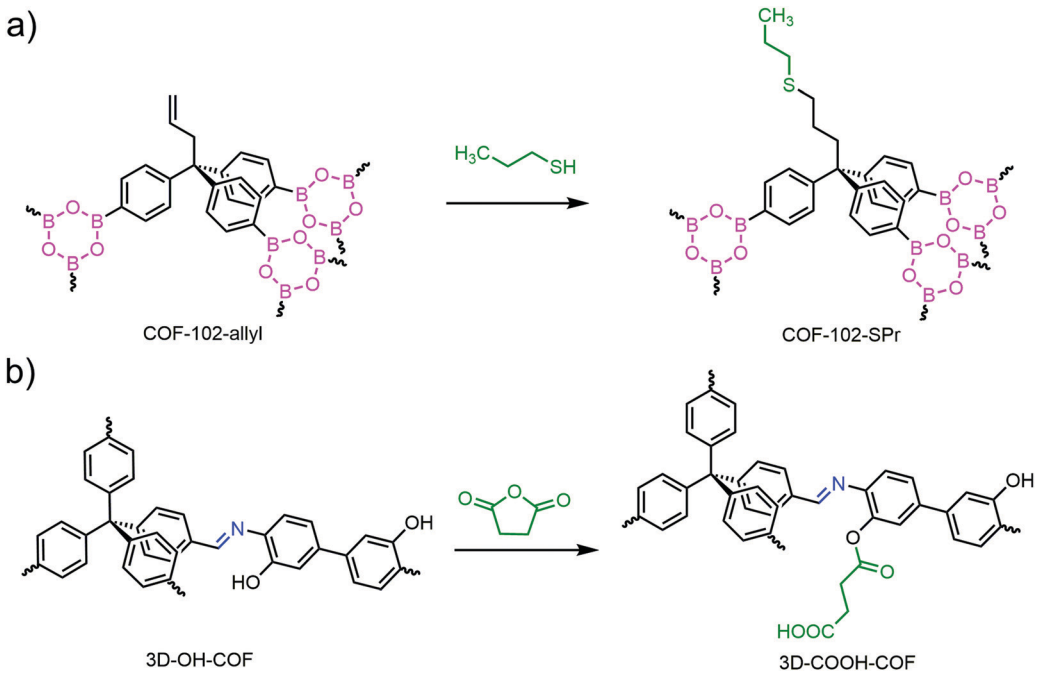

Fig. 10 (a) Post modification of COF-102-allyl by thiol–ene reaction. (b) Preparation of 3D-COOH-COF by ring opening reaction.

The imine linkage in CCOF 5 was transformed into amide with retention of crystallinity and permanent porosity as well as enhanced chemical stability (Fig. 11b). Linkage transformation has been well studied in 2D COFs and significantly enhanced chemical stability can be observed in most cases, yet only one successful example was reported for 3D COFs. The destruction of crystallinity and porosity during the modification might be the greatest challenge in the research and lots of efforts are still required in this field.

Apart from covalent modification, metalation of predesigned COFs was another common method for structural decoration. Various 3D COFs with different coordinative groups have been modified *via* this way. Ni decoration of DBA-3D-COF 1 with π-electron conjugated dehydrobenzoannulene (DBA) units was first reported in 2016 (Fig. 12a).[80] This COF scaffold contained DBA which has a tendency to form a strong metal complex with Ni(0). The decoration was performed by immersing DBA-3D-COF 1 in a toluene solution of $Ni(COD)_2$. Afterwards, the metal modified 3D salphen COFs (JUC-509-Mn, JUC-509-Cu and JUC-509-Eu) (Fig. 12b)[45] and 3D porphyrin COFs (PCOF-Fe and PCOF-Co) (Fig. 12c)[81] were also acquired by similar means.

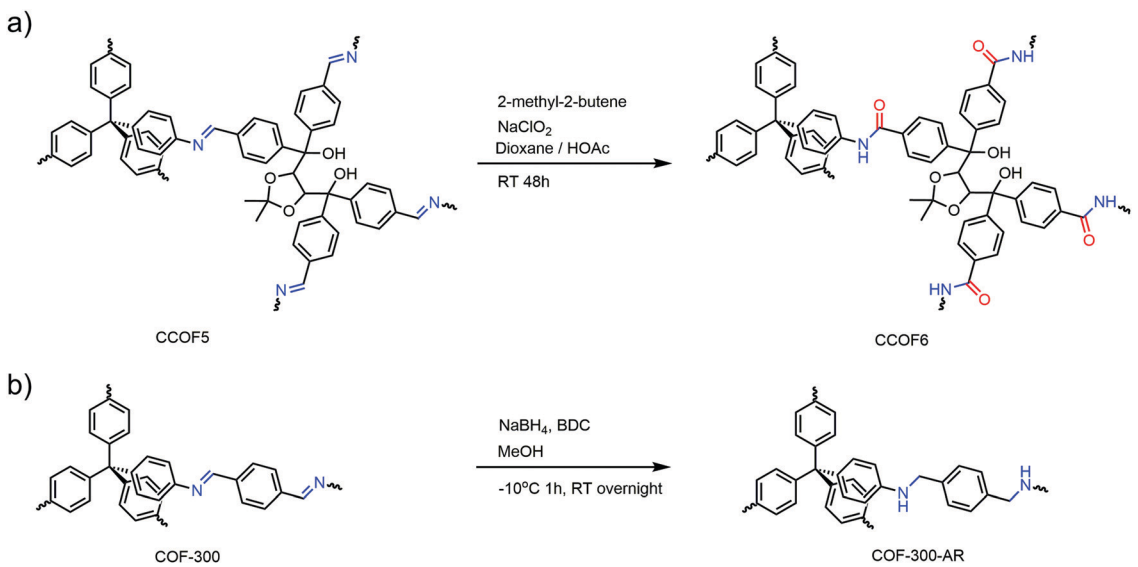

Fig. 11 Linkage transformation (a) from imine to amide in CCOFs and (b) from imine to amine in COF-300-AR.

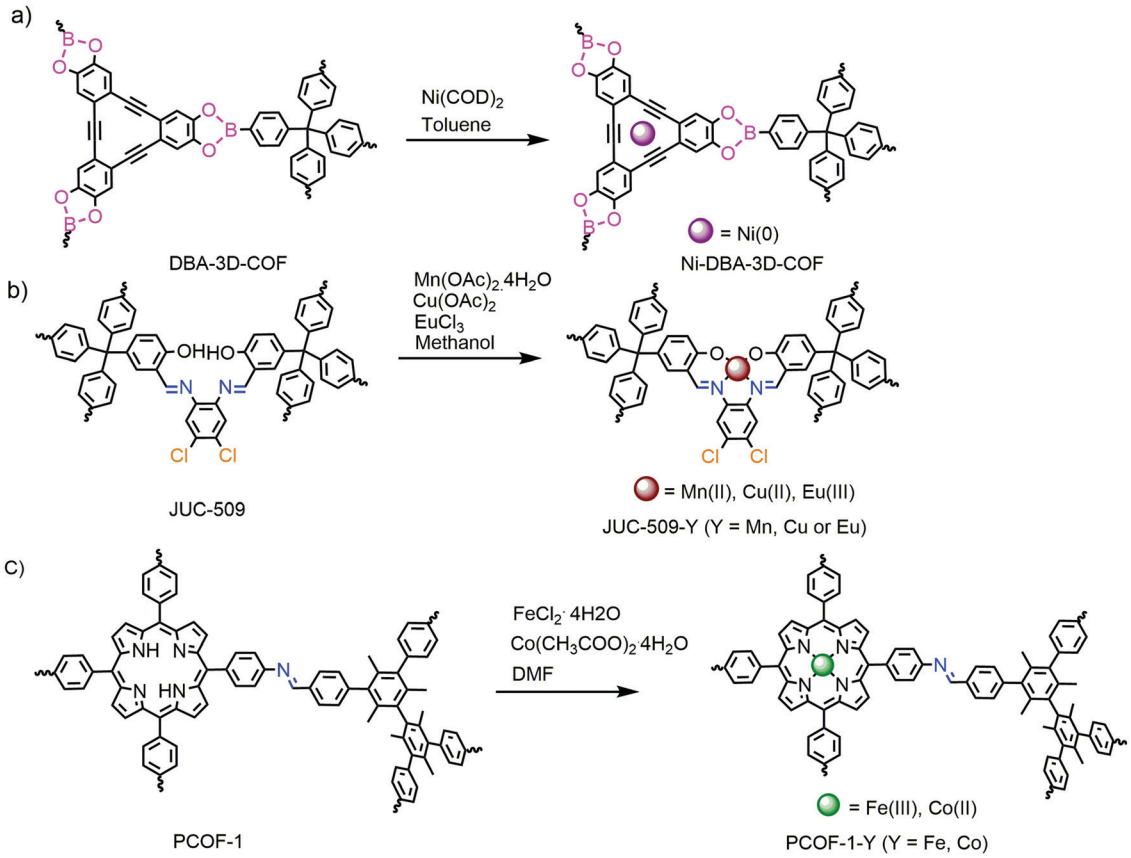

Fig. 12 The metalation of (a) DBA-3D-COF, (b) 3D salphen COFs, and (c) 3D porphyrin COFs.

The incorporation of small molecules or clusters into the channels was also useful in preparing functional 3D COFs. Weak interactions (including host–guest interactions, electrostatic interactions and van der Waals interactions) dominate the main forces of such procedures. In 2015, COF-300 was used as a support to immobilize phosphomolybdic acid (PMA) for getting novel hybrid PMA@COF-300 by a simple wetness impregnation method.[82] After that, 1-ethyl-3-methylimidazolium bis(trifluoromethylsulfonyl)imide ([Emim][Tf_2N]), a common ionic liquid, was also confined into the nanopores of COF-320.[83] Guest–host interactions between the ionic liquid and the COF scaffold were studied by complementary methods including FT-IR, differential scanning calorimetry (DSC) and solid-state ^{19}F NMR.

4 Applications of 3D COFs

4.1 Gas uptake

With a large void space, abundant open channels and sometimes exposed binding sites, 3D COFs are promising materials for gas uptake.

4.1.1 Hydrogen storage. Hydrogen (H_2) is an important clean energy carrier and it is still a great challenge to develop reasonably safe and reversible H_2 storage materials for transportation. As an ideal candidate for H_2 storage, 3D COFs demonstrate extremely high surface areas, low densities, and abundant open 3D channels. And more importantly, the entire material is accessible and an adsorbed molecule ''sees'' all the atoms of the framework.

In 2008, Yaghi and co-workers calculated the H_2 uptake of a series of COFs through grand canonical Monte Carlo (GCMC) simulations, and the simulated H_2 storage capacities of 3D COFs (COF-102, -103, -105, and -108) were 2.5–3 times higher than that in 2D materials.[84]

In the following year, Yaghi and co-workers measured the H_2 uptake behavior and capacity of COFs and other porous materials.[2] 3D COFs outperformed 2D COFs, and rivaled the best MOFs and other porous materials in their uptake capacities. With high BET surface areas (3620 $m^2\ g^{-1}$ for COF-102, 3530 $m^2\ g^{-1}$ for COF-103) and pore volume (1.55 $cm^3\ g^{-1}$ for COF-102, 1.54 $cm^3\ g^{-1}$ for COF-103), 3D COFs exhibited high saturation H_2 uptake (72.4 mg g^{-1} for COF-102 and 70.5 mg g^{-1} for COF-103 at 77 K and 35 bar), much exceeding that of 2D COFs (no more than 39.2 mg g^{-1} at 77 K and 35 bar). Similar results were obtained in the following works.[85,86]

Hydrogen adsorption sites and energies in 3D COFs were studied by molecular dynamics simulations in 2010.[87] For COF-102 and COF-103, the H_2 molecule preferred to be adsorbed vertically on the top of the benzene ring (with adsorption energies of −3.12 kJ mol^{-1} for COF-102 and −2.84 kJ mol^{-1} for COF-103),

while parallel on the top of the boron–oxygen ring (with adsorption energies of −1.96 kJ mol^{-1}). In addition, the side of the boron–oxygen ring was also a possible adsorption site (with an adsorption energy of −0.94 kJ mol^{-1}). The preferential hydrogen adsorption site on COF-105 and COF-108 was on the top of the outer three hydrocarbon rings (with adsorption energies of −1.95 kJ mol^{-1}) and on the side of the C_2O_2B ring (with adsorption energies of −2.30 kJ mol^{-1}). And the adsorption site in COF-202 was next to the Si–O–B cluster (with adsorption energies of −0.99 kJ mol^{-1}). These results were in good agreement with the previous work on 2D COFs.[88]

H_2 uptake capacities of 3D COFs can be enhanced by structural design. Froudakis and co-workers proposed a series of different 3D COFs based on COF-102 and studied their storage capacities by GCMC simulations.[89] COF-102-2, COF-102-3, COF-102-4, and COF-102-5 were devised by substituting the phenylene moieties of COF-102 with diphenyl, triphenyl, naphthalene, and pyrene without changing the net topology. The predicted total gravimetric adsorption of COF-102 was 9.95 wt% at 77 K and 100 bar, which was in line with the experimental results of just above 10 wt% under the same thermodynamic conditions. The proposed structures showed enhanced gravimetric capacities with respect to COF-102, at both cryogenic and room temperature. COF-102-3 showed the best performance and reached 26.7 and 6.5 wt% at 77 and 300 K at 100 bar, which exceeded the Department of Energy (DOE) target of 6 wt% even at room temperature.

Post-modification approaches such as Li-doping, impregnation, and functionalization are also promising methods to enhance H_2 adsorption in COFs. In 2009, Wang and co-workers studied the performance of four 3D COFs (COF-102, COF-103, COF-105 and COF-108) and their Li-doped derivatives through a multiscale theoretical method which combines first-principles calculations and GCMC simulation.[90] The calculations showed that COFs were superior to MOFs in H_2 storage. The H_2 gravimetric storage capacities of COF-105 and COF-108 reached 18.05 and 17.80 wt% at 77 K and 100 bar (approximately 10 wt% for MOFs under similar conditions). And the room-temperature H_2 storage capacities of COF-105 and COF-108 reached 4.67 and 4.51 wt% at 298 K and 100 bar. Furthermore, to meet the requirements for practical use in H_2 storage, 3D COFs were doped with Li atoms and the gravimetric adsorption capacities for H_2 in Li-doped COF-105 and COF-108 reached 6.84 and 6.73 wt% at 298 K and 100 bar. Similar results were obtained by Froudakis and co-workers for the lithium alkoxide COF which reached 22 wt% and 51 g L^{-1} at 77 K and 100 bar, and reached the DOE target for gravimetric uptake (6 wt%) even at room temperature.[91] Similar results were also obtained for borosilicate COF-202.[92] 3D COFs with Li–Sc doping,[93] Li–C60 doping[94] and other metal dopings[95,96] were modelled and predicted for enhancing H_2 uptake afterwards.

4.1.2 Methane storage. Methane (CH_4, Nature Gas), another clean energy carrier, is considered as a possible alternative to petroleum due to its growing availability and potentially lower greenhouse gas emissions. The main drawback of NG is the low energy density under ambient conditions, and adsorbed natural gas (ANG) is one novel method for the densification and storage of NG. 3D COFs are particularly attractive ANG storage materials due to their low densities, high surface areas and large void space. But research is still limited in this field.

Yaghi and co-workers studied the CH_4 storage capacities of 3D COFs and compared with 2D structures and other porous materials in 2009.[2] In this work, two 3D COFs revealed remarkable CH_4 uptake capacities at 298 K at 35 bar (187 mg g^{-1} for COF-102 and 175 mg g^{-1} for COF-103) and 85 bar (243 mg g^{-1} for COF-102 and 229 mg g^{-1} for COF-103), much exceeding that of five 2D COFs (no more than 89 mg g^{-1} at 35 bar and 127 mg g^{-1} at 85 bar) and matching the best of other porous materials (*e.g.* 250 mg g^{-1} for anthracite at 293 K at 35 bar and 253 mg g^{-1} for PCN-14 at 290 K at 35 bar).

The adsorption mechanism and uptake of CH_4 in COFs were further studied by Yaghi and co-workers.[97] The CH_4 uptake was predicted from GCMC simulations based on force fields (FF) developed to fit accurate quantum mechanics (QM) for both 2D (COF-1, COF-5, COF-6, COF-8, and COF-10) and 3D (COF-102, COF-103, COF-105, and COF-108). Although the best COF in terms of total volume of CH_4 per unit volume of COF absorbent was COF-1, the best COFs on a delivery amount basis (volume adsorbed from 5 to 100 bar) were COF-102 and COF-103 with values of 229 and 234 v(STP: 298 K, 1.01 bar)/v, suggesting that they were suitable for practical applications of CH_4 storage.

Li-Doping was also employed for enhancing CH_4 uptake. Cao and co-workers studied the CH_4 uptake of Li-doped 3D COFs by using a multiscale theoretical method which combines the first-principles calculation and GCMC simulation.[98] The first-principles calculations showed that the Li cation doped in the COFs can enhance the binding of CH_4 significantly because of the London dispersion and the induced dipole interaction, due to the strong affinity of the Li cation to CH_4 molecules. At 298 K and relatively low pressure, Li-doped 3D COFs showed almost double CH_4 uptake (303 and 290 v(STP)/v for Li-doped COF-102 and COF-103 at 298 K and 35 bar) than those in the non-doped frameworks (127 and 108 v(STP)/v for COF-102 and COF-103 at 298 K and 35 bar).

Covalent modification was another approach for improving CH_4 capacity. Goddard and co-workers designed 14 new alkyl substituents containing COFs based on COF-102, COF-103, COF-105, COF-108 and COF-202.[99] The volumetric CH_4 delivery of two new frameworks, COF-103-Eth-trans (192 v(STP)/v) and COF-102-Ant (180 v(STP)/v), was found to exceed the DOE target of 180 v(STP)/v at 35 bar for CH_4 storage. Their performance was comparable to that of the best previously reported materials: PCN-14 and Ni-MOF-74 (112 v(STP)/v).

In 2018, a database of 69 840 COFs (including 18 813 interpenetrated 3D structures and 42 386 non-interpenetrated 3D structures) was assembled *in silico* from 666 distinct organic linkers and four established synthetic routes and their CH_4 uptake performances were studied.[100] Generally, 3D COFs demonstrated higher uptake than 2D COFs, because of the stronger adsorption sites (*e.g.*, binding pockets *vs.* layers). The highest delivery capacity reached 216.8 v(STP)/v at 65 bar, much higher than current MOFs and COFs (197 v(STP)/v at 65 bar for Co(bdp)

and 203 v(STP)/v at 80 bar for COF-102). The influence of topologies and linkages was further studied. The **qzd**, **pth**, and **pts** nets tended to be the top performing CH_4 materials in the C–N bonded structures, whereas **ukk**, **uon**, and **dia** were the most common nets in the best C–C bonded structures. It was interesting that the **sql** net was in the majority of the best performing C–N structures, but also in the majority of the worst C–C bonded structures. This phenomenon was attributed to the longer length of the C–N bond than the C–C bond, which means the optimal CH_4 storage densities of the C–N bonded structures were shifted to suboptimal values when the C–N bonds were replaced with C–C bonds.

4.1.3 Carbon dioxide capture. As the major greenhouse gas and a potential carbon source, the capture and separation of carbon dioxide (CO_2) is in the focus of energy and environment related concerns. 3D COFs with abundant channel structures and accessible binding sites are attractive in this field.

Again in the report of Yaghi in 2009, CO_2 capture capacity was measured for the first time for 3D COFs.[2] High CO_2 capacity of COF-102 (1200 mg g^{-1}) and COF-103 (1190 mg g^{-1}) at 298 K and 55 bar was observed. The performance of some 2D COFs and other porous materials was also studied in this paper. 3D COFs performed better than the 2D network under the same conditions (no more than 1010 mg g^{-1}) but a little inferior to some MOFs (*e.g.* 1490 mg g^{-1} for MOF-177 at 298 K at 40 bar and 1760 mg g^{-1} for PCN-14 at 298 K at 50 bar).

In 2017, Zhang and co-workers studied the influence of relative humidity (RH) over CO_2 uptake in the dynamic 3D COF LZU-301.[101] Breakthrough experiments using CO_2/N_2 gas mixtures (v/v = 10 : 90 at 298 K and 1 bar) under dry or humid conditions were employed and different capacities were obtained for different RH (0.22 mmol g^{-1} under dry conditions, 0.29 mmol g^{-1} under 17% RH and 0.37 mmol g^{-1} under 83% RH). It is notable that the value under 83% RH was even higher than the CO_2 uptake (0.35 mmol g^{-1}) of the activated framework at 298 K and $P/P_0 = 0.1$, indicating a gate-open effect in the presence of water.

4.1.4 Iodine capture. Iodine (^{129}I and ^{131}I) is a major radioactive waste vapour and the adsorption of iodine using porous materials has attracted increasing attention in recent years. Gao and co-workers employed a new 3D COF (COF-DL229) as a porous platform for removing iodine vapor in 2018.[47] COF-DL229 achieved an uptake capacity of 82.4 wt% (1 g COF-DL229 adsorbed 4.7 g iodine) at 75 °C, surpassing other porous materials based on inherent porosity (*e.g.* 82.4 wt% for COF-320 and 73.4 wt% for PAF-24). Moreover, COF-DL229 exhibited an excellent performance even in open air and ambient conditions (70.0 wt%). More interestingly, iodine-loaded I_2@COF-DL229 samples exhibited high retention capacity (the loss of loaded iodine started at 131 °C and completed at 300 °C) and ultrafast release performance in methanol (the release rate constant was 2.02×10^{14}, 3.03×10^{12}, and 2.47×10^{11} I_2 s^{-1} for samples at 30 s, 5 min, and 60 min). Moreover, the porous skeleton of COF-DL229 was "soft" to trigger structural fitting to iodine while retaining the covalent connectivity and enabled repeated use many times while retaining high uptake capacity (66 wt% after the first cycle and 63 wt% after another three cycles).

The gaseous I_2 and CH_3I adsorption was also measured with 187 experimentally reported COFs.[102] 3D COFs presented better performance than 2D COFs for both I_2 and CH_3I adsorption and 3D-Py-COF exhibited the highest I_2 uptake of 16.7 g g^{-1}, outperforming the adsorbents reported to date. Furthermore, a new 3D-COF with an even higher I_2 uptake of 19.9 g g^{-1} was designed by replacing TAPM in 3D-Py-COF by tetra(*p*-amino naphthyl) methane (TANM). For CH_3I adsorption, the pore morphology played an important role, and five 3D-COFs with ctn topology with a pore size of around 9 Å showed the best performance among the 187 COFs. COF-103 was the best material with a CH_3I uptake of 2.8 g g^{-1}, which was much higher than those of traditional adsorbents like activated carbons (0.32 g g^{-1}), alumina (0.22 g g^{-1}) and zeolites (0.10 g g^{-1}).

4.2 Gas separation

4.2.1 Hydrogen separation. A COF-320 membrane on the porous α-Al_2O_3 support was used for H_2 separation for the first time.[69] The H_2 permeation flux was relatively high compared to that of CH_4 and N_2, indicating that the COF-320 membrane is H_2 selective with a high H_2 permeance of 5.67×10^{-7} mol $(m^2\ s\ Pa)^{-1}$. The permselectivity for H_2/CH_4 and H_2/N_2 was about 2.5 and 3.5, respectively, and the ideal separation factor was closely similar to those (2.83 for H_2/CH_4, 3.74 for H_2/N_2) theoretically calculated by the Knudsen diffusion mechanism. The gas permeation results indicated that the gas transport behavior was mainly governed by the predicted Knudsen diffusion process due to the large nanopores of 3D COF-320.

The COF-300/MOF hybrid membranes reported by Ben were also applied for H_2 separation.[70] The mixture separation factors of a H_2/CO_2 (1 : 1) binary mixture through the [COF-300]-[Zn_2(bdc)$_2$(dabco)] (12.6) and [COF-300]-[ZIF-8] (13.5) composite membranes were much higher than that of COF-300 (6.0), Zn_2(bdc)$_2$(dabco) (7.0), and ZIF-8 (9.1) membranes. The separation factors were higher than the Robeson upper bound limit of gas separation by polymer membranes. This remarkable performance was due to the formation of chemical bonds between different components (support, COF, and MOF), including imine groups between the COF crystals and polyaniline layer and HN-Zn-imidazole bonds at the interface between COF and ZIF materials.

4.2.2 Carbon dioxide separation. The general strategy for boosting selective CO_2 capture performance is by introducing some moieties with high CO_2 affinity into porous materials. In the following report by Fang and co-workers, ILs were introduced into the channel of 3D COFs by *in situ* room-temperature ionothermal synthesis.[55] 3D-IL-COFs obtained from [BMIm][NTf_2] exhibited high CO_2 capture and separation performance due to rich channels and strong interactions between ILs and CO_2. The CO_2 uptake of 3D COFs with [BMIm][NTf_2] at 298 K and 1 bar (5.34%, 7.61% and 4.93% for three 3D-IL-COFs respectively) was much higher than CH_4 (0.37%, 0.85% and 0.33%) and N_2 (0.35%, 0.51% and 0.28%) uptake measured under the same conditions. A high CO_2/N_2 and CO_2/CH_4 adsorption selectivity was observed (24.6 and 23.1 in 3D-IL-COF-1, 24.0 and 22.3 in 3D-IL-COF-2, and 24.4 and 21.5 in 3D-IL-COF-3). In contrast, 3D-IL-COF-1a, the isomer of

3D-IL-COF-1 but without [BMIm][NTf_2], exhibited relatively low selectivity (7.1 for CO_2/N_2 and 5.3 for CO_2/CH_4). However, the selectivity can be further improved (43.6 for CO_2/N_2 and 35.1 for CO_2/CH_4) by using [BMIm][$N(CN)_2$], another ionic liquid which possessed higher CO_2 affinity than [BMIm][NTf_2]. Moreover, the high CO_2 separation performance of 3D-IL-COF-1 was further confirmed by breakthrough measurements.

In 2019, Sun and co-workers studied the influence of the pore environment over selective sorption capabilities.[103] In this work, the selective sorption of CO_2 over N_2 was investigated for a series of isostructural 3D COFs with similar crystallinity and topology and different substituents (3D-TPB-COF-H, 3D-TPB-COF-Me and 3D-TPB-COF-F). These frameworks exhibited very low N_2 uptake but much higher CO_2 adsorption (about 90 $cm^3\ g^{-1}$ for all three COFs) at 273 K and 1 bar. However, higher adsorption at low CO_2 pressure and greater isosteric heats of adsorption (Q_{st}) were observed for 3D-TPB-COF-F (28.4 kJ mol^{-1}) than 3D-TPB-COF-H (21.8 kJ mol^{-1}) and 3D-TPB-COF-Me (24.7 kJ mol^{-1}). The adsorption selectivity for CO_2/N_2 mixtures (15 : 85) was calculated based on ideal adsorbed solution theory (IAST) as 50 for 3D-TPB-COF-F at 1 bar, much higher than 24 for 3D-TPB-COF-H and 31 for 3D-TPB-COF-Me.

Other than powders, COF-300-based MMMs were also used for CO_2 separation.[71] Due to the fast gas transport paths from the highly porous 3D COF fillers, 6FDA-DAM and Pebax systems demonstrate 52% and 57% increase in CO_2 permeability respectively. Meanwhile, gas molecules can be discriminated based on the ultrasmall 4 Å pores in COF-300 and increased selectivity of smaller gas molecules (*e.g.* CO_2) over larger ones (*e.g.* CH_4 or N_2) was achieved. In contrast, a slightly increased or even decreased selectivity was observed for MMMs containing 2D COFs with relatively large pores (> 8 Å).

4.2.3 Separation of ethane and ethylene. Ethylene is one of the most important chemicals and the adsorption and separation of ethane and ethylene is an essential process in petrochemistry. As a class of crystalline porous materials, 3D COFs possess high potential in gas uptake and separation with their unique structures and properties. The uptake capacities and separation performance of DBA-3D-COF 1 and its nickel derivatives (Ni-DBA-3D-COF) were investigated by McGrier and co-workers in 2016.[80] DBA-3D-COF 1 exhibited a swift uptake at low pressures and demonstrated an uptake of 3.24 mmol g^{-1} at 273 K and 2.09 mmol g^{-1} at 295 K for ethane and 2.52 mmol g^{-1} at 273 K and 1.70 mmol g^{-1} at 295 K for ethylene. In comparison, Ni-DBA-3D-COF displayed uptake capacities of 3.01 and 2.16 mmol g^{-1} for ethane and 2.36 and 1.83 mmol g^{-1} for ethylene at 273 and 295 K, respectively. The uptake capacities of Ni-DBA-3D-COF only increased slightly by 0.07 mmol g^{-1} for ethane and 0.13 mmol g^{-1} for ethylene at 295 K. The ethane/ethylene selectivity of DBA-3D-COF 1 and Ni-DBA-3D-COF was calculated as 1.25 and 1.28 at 273 K, and 1.24 and 1.15 at 295 K, respectively.

4.3 Adsorption and separation in the liquid phase

Ample open channels, large surface areas, easily accessible binding sites as well as high chemical stability make 3D COFs excellent materials for adsorption in the liquid phase.

4.3.1 Dye removal. Owing to lots of easily accessible void space, good affinity to many organic dyes and excellent chemical stability, 3D COFs are good materials for removal of dyes from solutions.

The first work in this field was conducted in 2012.[73] The solvatochromic dye pyridinium iodide was loaded in pristine COF-102 and dodecyl-functionalized COF-102-C_{12}, which was confirmed by diffuse reflectance UV/vis spectra.

In 2017, Fang and co-workers chose two 3D ionic COFs (3D-ionic-COF-1 and 3D-ionic-COF-2) for inclusion of two organic dyes with different sizes.[44] The methyl orange (MO, 5.4 × 7.8 × 15.2 Å) which is smaller than the channel of 3D-ionic-COFs (8.6 Å for 3D-ionic-COF-1 and 8.2 Å for 3D-ionic-COF-2) was almost completely captured in about 20 min but methyl blue (MB, 13.9 × 14.4 × 24.5 Å) remained in the solution, which confirmed the size discrimination ability of 3D-ionic-COFs.

The removal studies of three anionic fluorescent dyes of increasing size (MO < HN < MB) were also carried out with two 3D woven COFs (non-interpenetrated COF-506-Cu with pore width 11.1 × 15.2 Å and double-interpenetrated COF-505-Cu) (Fig. 13).[104] As the size of the dye increased, MO and HN were only adsorbed by COF-506-Cu but almost no uptake of MB was observed in both frameworks. Interestingly, the demetalated COF-506 exhibited a major uptake of MB, 11.6-fold higher than that of its metalated analogue, thus giving credence to a novel mode of motional dynamics in solids termed as 'adaptive inclusion'.

4.3.2 Ion exchange. The removal of different ions from solutions with high efficiency and selectivity is also pretty meaningful under special occasions. In the same report by Fang and co-workers,[44] 3D ionic COFs were also used to remove MnO_4^-, the model compound of radioactive technetium (Tc-99). Almost 100% removal of MnO_4^- was observed in 20 min, much exceeding the performance of other ion-exchange materials including PVBTAH-ZIF-813 and LDHs. The crystal structures were preserved after ion exchange as confirmed by PXRD and N_2 adsorption analysis, and COF crystals can be easily recycled and reused at least five times with almost no loss of activity.

And in another work of Fang and co-workers, a 3D carboxyl-functionalized COF (3D-COOH-COF) was designed which displayed high metal loading capacities together with excellent adsorption selectivity for Nd^{3+} over Sr^{2+} and Fe^{3+} (Fig. 14).[78] The extraction capability of 3D-COOH-COF was studied by Langmuir adsorption isotherms. The much higher Langmuir parameter *b* for Nd^{3+} (15.87 mM^{-1}) than for Sr^{2+} (0.85 mM^{-1}) and Fe^{3+} (0.08 mM^{-1}) ions suggested stronger adsorption in 3D-COOH-COF for Nd^{3+} than for Sr^{2+} and Fe^{3+}, which was consistent with the highest uptake for Nd^{3+} at low concentration.

4.3.3 Drug delivery. Many drugs have a short biological half-life and need sustained or controlled drug delivery. With a good affinity to drug molecules and high stability, 3D COFs are ideal for the controlled release of drugs. In the paper reported by Fang and co-workers in 2015, two 3D PI-COFs (PI-COF-4 and PI-COF-5) were employed to control Ibuprofen (IBU) delivery

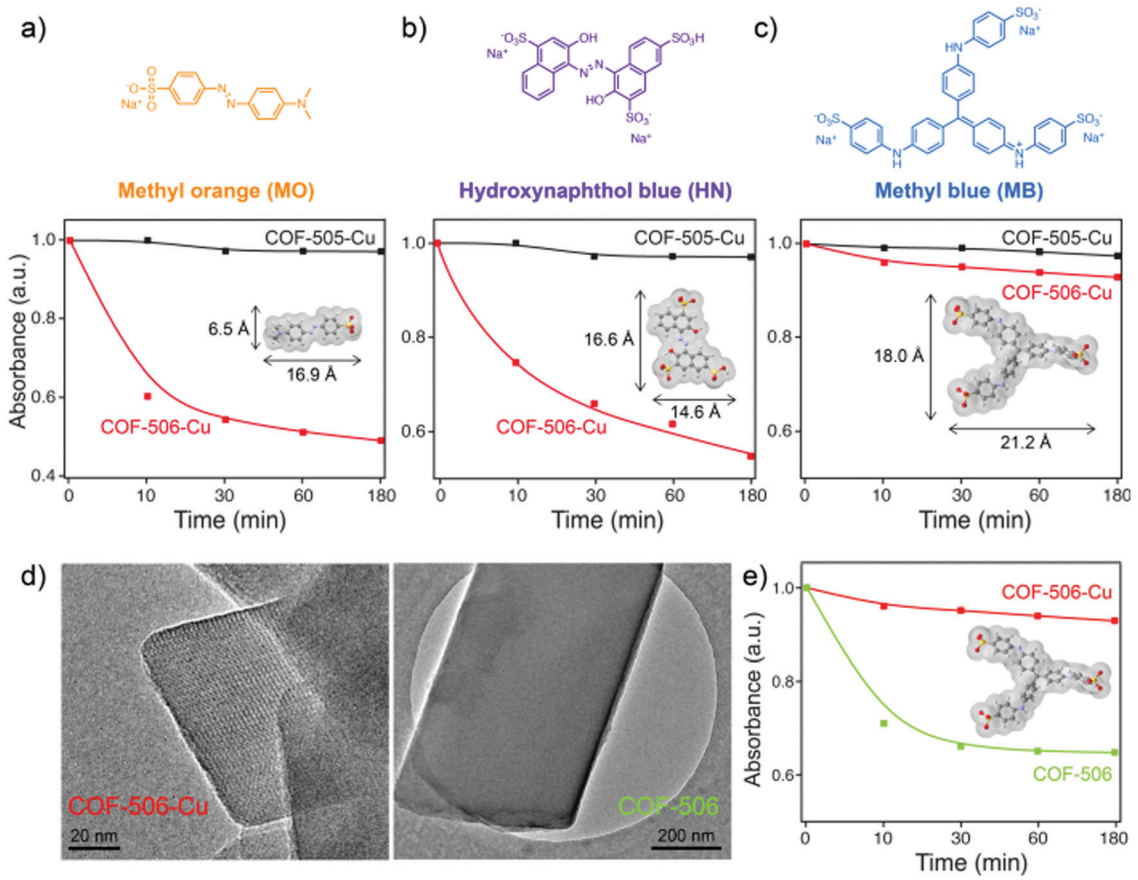

Fig. 13 Dye uptake of 3D woven COFs (reproduced from ref. 104 with permission from American Chemical Society, Copyright 2018).

in vitro (Fig. 15).[25] After immersing PI-COFs in IBU hexane solution and stirring for 2 h, IBU contents were evaluated as 24 and 20 wt% in PI-COF-4 and PI-COF-5 based on thermogravimetric analysis (TGA). For both PI-COFs, the majority of the IBU was released after about 6 days, and total delivery could reach *ca.* 95% of the initial IBU loading. However, PI-COF-5 with a smaller pore size (13 Å for PICOF-4 and 10 Å for PI-COF-5) showed a lower release rate (*e.g.*, 60% for PI-COF-4 *vs.* 49% for PI-COF-5 after 12 h), indicating that the drug delivery in COFs was directly related to the pore size and geometry. Moreover, the controlled release tests were also conducted over two other drugs, namely, captopril and caffeine. The results showed that COFs loaded with these drugs also have good release control.

4.3.4 Chromatographic separation. Considering the insoluble nature, high chemical stability and good adsorption selectivity of 3D COFs, these materials have the potential to become the stationary phase of chromatography. In 2018, Liu and co-workers used two chiral 3D COFs (CCOF 5 and CCOF 6) as the stationary phases for high performance liquid chromatography to enantioseparate racemic alcohols.[50] The column packed with CCOF 5 baseline separated racemic 1-phenyl-2-propanol successfully but failed for racemic 1-phenyl-1-pentanol, 1-phenyl-1-propanol and 1-(4-bromophenyl)-ethanol (Fig. 16). In contrast, the column packed with CCOF 6 could baseline resolve all of the four racemic alcohols. Other types of racemates such as sulfoxides, carboxylic acids and esters can also be completely or partly resolved. In all cases, CCOF 6 showed an improved resolution ability compared to CCOF 5 under similar conditions. No separation for 1-(1-naphthyl)-ethanol with a minimum diameter of 0.85 nm (larger than 0.71 nm for CCOF-5 and 0.75 nm for CCOF-6) was observed, confirming that the resolution abilities of the CCOFs are likely to come from the chiral channels. As controls, monodispersed amorphous COF@SiO_2 and (R,R)-TTA/SiO_2 hybrid microspheres were prepared but they could not separate racemic alcohols, further highlighting the key role of the crystalline 3D structure in chiral recognition.

C_8 alkylaromatic isomers (*o*-xylene, *m*-xylene, and *p*-xylene and ethylbenzene) are important raw materials but are often obtained as mixtures. The separation of C8 alkylaromatic isomers is difficult but an important task in petrochemistry. Cui and co-workers utilized four 3D Salen COFs as the stationary phase in high performance liquid chromatography (HPLC) columns for the separation of ethylbenzene and xylene isomers.[48] Both COF 1 and COF 2 can give high-through separation of EB and xylene isomers, but COF 1-Zn and COF 2-Zn cannot offer baseline separation. This indicated the importance of uncoordinated polar salen units in isomer recognition and separation. During the separation, ethylbenzene and *p*-xylene came out first due to their lowest dipole moment,

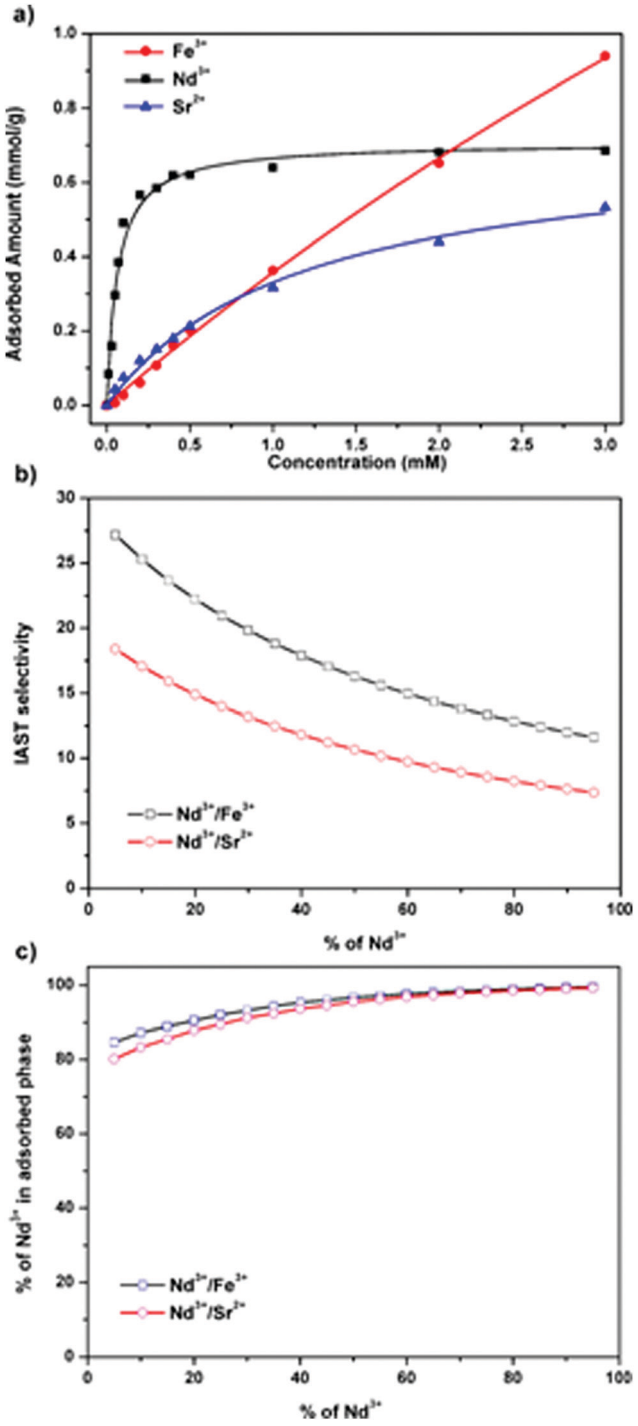

Fig. 14 Ion exchange performance of 3D-COOH-COF (reproduced from ref. 78 with permission from Wiley-VCH, Copyright 2018).

followed by *m*-xylene that can only interact with the salen units with one methyl group. More interestingly, good separation was achieved for five more isomer mixtures. Similar to the last work, almost no separation was achieved for substrates with sizes larger than the pore width or with monodispersed amorphous COF 1/SiO_2 hybrid particles and COF 1@SiO_2 shell–core particles, indicating that analyte recognition happened in crystalline microporous channels.

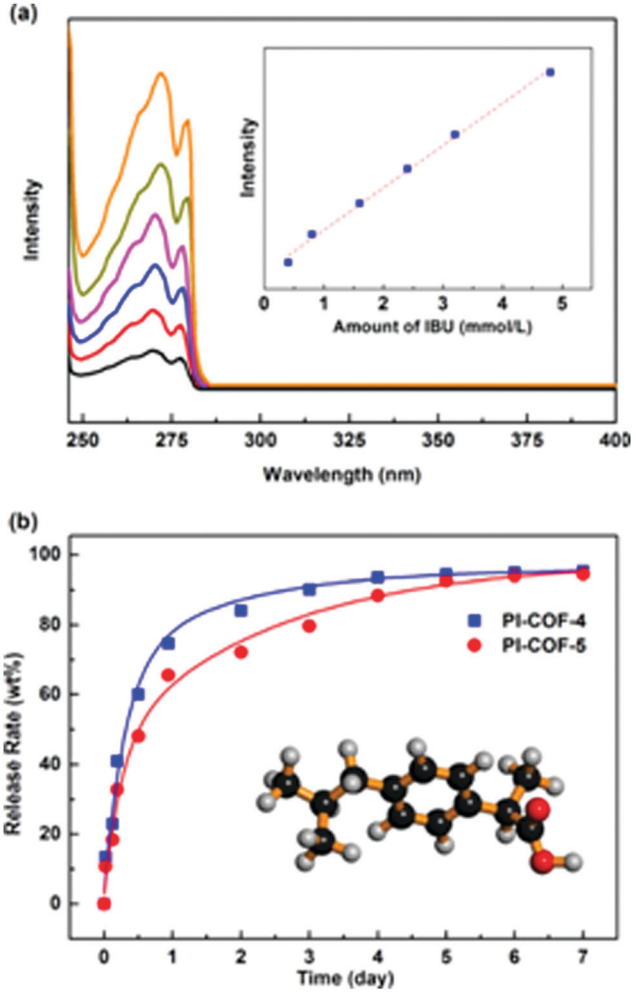

Fig. 15 Drug delivery performance of 3D PI-COFs (reproduced from ref. 25 with permission from American Chemical Society, Copyright 2015).

4.4 Heterogeneous catalysis

3D COFs are promising platforms for catalysis. Abundant uniform open channels in 3D networks are vital for the mass transfer process in catalysis and can provide some interesting properties like size-selectivity. The insolubility nature and high stability confirm the easy isolation from reaction mixtures and good reusability of catalysts. More importantly, various accessible active sites can be further anchored precisely onto the channels by *in situ*, pre-modification or post-functionalization approaches.

The first kind of catalytic centers were from linkages in 3D COFs. Schiff bases generated in imine COFs are alkaline and can serve as base-catalytic active sites. In 2014, two TAA-based 3D COFs (BF-COF-1 and BF-COF-2) were employed as highly efficient and size-selective catalysts for the first time (Fig. 17).[40] In the article, the researchers found that COFs constructed from alkyl amines demonstrated strong basicity and could be promising base catalysts. The classical base-catalyzed Knoevenagel condensation reaction was conducted under the catalysis of both BF-COFs, and high conversions (96% for BF-COF-1 and 98% for BF-COF-2) were observed for suitable substrates.

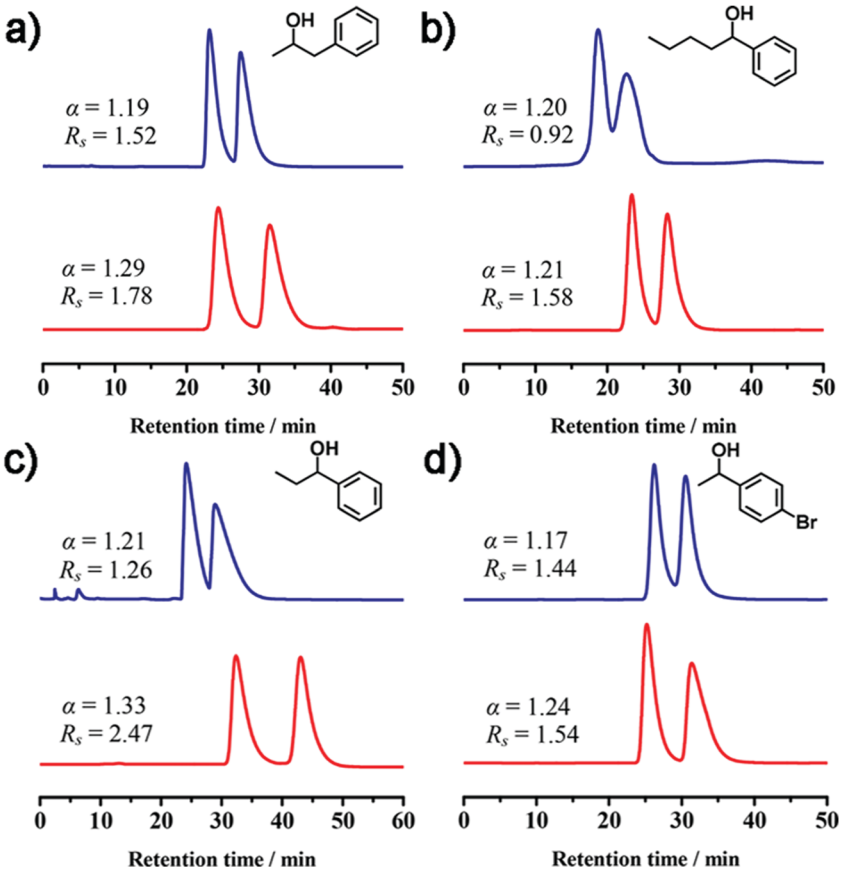

Fig. 16 Separation performance of racemic alcohols with CCOF 5 (blue line) and 6 (red line) as the stationary phase of chromatography (reproduced from ref. 50 with permission from American Chemical Society, Copyright 2018).

Meanwhile, owing to the uniform pores of the frameworks, these materials exhibited highly efficient size selectivity. Furthermore, as heterogeneous catalysts, these COFs can be readily isolated from the reaction suspension by simple filtration and reused almost without loss of activity at least three times.

Other than Schiff bases, boroxine rings can act as acid-catalytic centres in COFs. In the following report, Fang and co-workers designed two 3D COFs (DL-COF-1 and DL-COF-2) based on dual linkages.[72] With Schiff bases as basic sites and boroxine rings as acidic sites, the catalytic potential of DL-COFs for the acid–base catalyzed one-pot cascade reactions was explored. By choosing hydrolysis of the acetal as the acid-catalyzed reaction followed by Knoevenagel condensation as the base-catalyzed reaction, high yield of the final product was observed for both COF catalysts and wide substrates, confirming the high activity for the cascade reactions. Also, the COF crystals can be isolated easily and reused at least three times with almost no loss of activity.

Furthermore, COF-300-AR with amine linkage was used for electrochemical selective reduction of CO_2. Compared with the COF on the bare silver electrode, the COF on the silver electrode exhibited an increased faradaic efficiency (FE) of CO from 13% to 53% and 43% to 80% under the potential of 0.70 and 0.85 V *versus* RHE while the HER was obviously suppressed from 80% to 22% and 60% to 9% under 0.70 and 0.85 V *versus* RHE, respectively. No obvious improvement in CO_2 conversion selectivity was observed on the silver electrode decorated with only Nafion binder or COF-300, and almost no CO_2 conversion took place on the glassy carbon electrode using COF-300-AR. Physisorption and diffusion of CO_2 in pores, strong interactions between amine and CO_2 as well as the formation of carbamate might be the possible mechanism.

Salphen, an important organo-metallic catalyst, has also been introduced into 3D COFs. In 2019, Fang and co-workers reported the design and preparation of two 3D-salphen-COFs (JUC-508 and JUC-509) and their metal derivatives (3D-M-salphen-COFs).[45] JUC-509 and its metal derivatives (JUC-509-Cu, JUC-509-Mn, JUC-509-Eu) were employed to catalyze the dismutation of the superoxide radical anion. JUC-509 and JUC-509-Eu exhibited no obvious activity, but JUC-509-Cu demonstrated good performance (almost 100% clearance rate at only 0.875 mg mL^{-1}). More importantly, these COF catalysts can be readily recycled and reused at least three times without obvious loss of activity.

Catalytic sites can also be incorporated in 3D COFs by employing those building blocks with functional moieties. With pyridyl moieties in the channels, LZU-301 was reported as another solid base catalyst for Knoevenagel condensation reactions.[101] For the conversion from benzaldehyde (6.5 × 8.5 $Å^2$) to benzylidenemalononitrile (8.0 × 11.3 $Å^2$), 72% yield in 6 h and

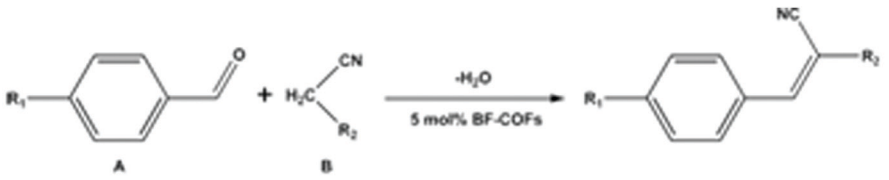

entry	A	B	catalyst	conversion (%)
(a)	8.7 Å, 6.1 Å	6.9 Å, 4.5 Å	BF-COF-1	96
			BF-COF-2	98
(b)	13.3 Å, 6.1 Å	6.9 Å, 4.5 Å	BF-COF-1	3
			BF-COF-2	4
(c)	8.7 Å, 6.1 Å	10.3 Å, 5.8 Å	BF-COF-1	3
			BF-COF-2	3
(d)	13.3 Å, 6.1 Å	10.3 Å, 5.8 Å	BF-COF-1	2
			BF-COF-2	3

Fig. 17 Heterogeneous catalysis performance of BF-COFs (reproduced from ref. 40 with permission from Wiley-VCH, Copyright 2014).

99% yield in 10 h were observed for LZU-301, outperforming COF-320 (42% yield in 6 h) and nonporous analogue LZU-101 (21% in 6 h). Lower activities and yields were observed for those substrates with oversize products, indicating the size-selective effect of 3D frameworks.

Porphyrin and its metal derivatives are an important class of photocatalysts. In 2017, Wang and co-workers prepared two photosensitive 3D porphyrin-based COFs (3D-Por-COF and 3D-CuPor-COF) and employed them as heterogeneous catalysts for generating singlet oxygen under photoirradiation with 9,10-dimethylanthracene (DMA) as the label (Fig. 18).[75] 3D-CuPor-COF exhibited weaker photocatalytic activity (45% DMA was still left after photoirradiation for 12 h) compared with 3D-Por-COF (99% DMA degraded after photoirradiation for 90 min under the same conditions), in line with the previous research that porphyrins containing paramagnetic metal ions were poor photosensitizers. These results suggested that the properties of 3D porphyrin-based COFs can be tuned by metalation of porphyrin rings. Interestingly, high activity was still present with degradation efficiency up to 94% after three cycles for 3D-Por-COF. Two years later, Wang and co-workers further compared 2D and 3D porphyrin-based COFs and found better photocatalytic performance and size-selective photocatalysis for 3D structures.[76] In this research, a 3D COF (3D-PdPor-COF) and a 2D COF (2D-PdPor-COF) were synthesized using the same porphyrin-based monomer (p-PdPor-CHO). Considering the good photosensitization of palladium porphyrins, significantly different alignments of palladium porphyrins in these two COFs and the smaller pore size of 3D-PdPor-COF, visible-light-induced aerobic oxidation of thioanisole to methyl phenyl sulfoxide was chosen as the model reaction. 3D-PdPor-COF can reach a yield of 98% in 0.4 h and was still highly active after 3 runs without any special treatment, which was comparable to many reported heterogeneous photocatalysts and much better than the yield of only 48% when using 2D-PdPor-COF as the photocatalyst under the same conditions. To investigate the size-selective effect of the frameworks, substrates with different sizes were studied. For small substrates, 3D-PdPor-COF exhibited higher yields than 2D-PdPor-COF under the same conditions. Hence the performance of 3D-PdPor-COF decreased sharply (*e.g.* 48% for tert-butylphenyl methyl sulfide) while 2D-PdPor-COF still showed a reasonable yield (59%) when large substrates were used. A significant size-selective effect was observed for the 3D network as a result of smaller pore size.

Porphyrin is also a good biomimetic catalyst and electrocatalyst. Two 3D porphyrin COFs (PCOF-1 and PCOF-2) were synthesized as promising candidates for single-site catalysis.[81] The Fe derivatives exhibited excellent biocatalytic performance with k_{cat} of 23.4 min^{-1} for PCOF-1-Fe (ratio of metallization was 91%) and 3.96 min^{-1} for PCOF-1-Fe (ratio of metallization was 93%)

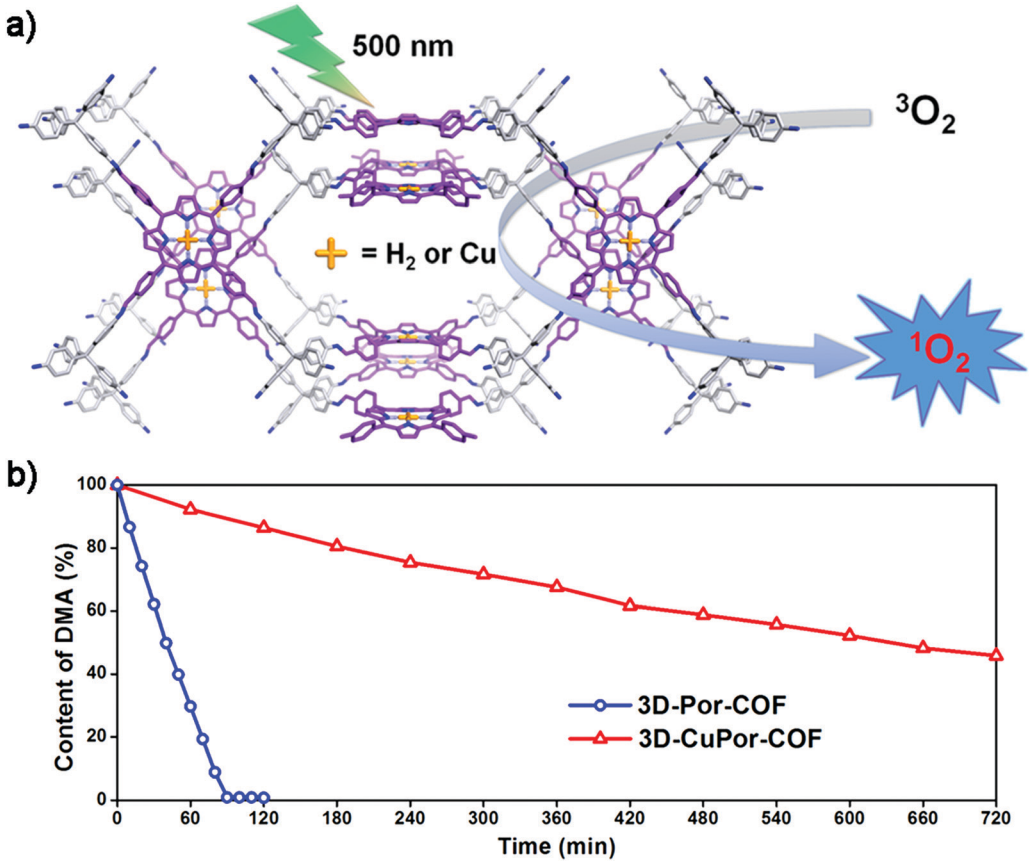

Fig. 18 (a) Schematic representation of 3D-Por-COF and 3D-CuPor-COF as heterogeneous catalysts for generating singlet oxygen. (b) Concentration irradiation time plots of 9,10-dimethylanthracene (DMA) (reproduced from ref. 75 with permission from American Chemical Society, Copyright 2017).

for the oxidation reaction of 2,2′-azinodi(3-ethylbenzothiazoline)-6-sulfonate (ABTS) with $ABTS^+$. The catalytic efficiency of PCOF-1-Fe ($k_{cat}/K_m \approx 1.5 \times 10^4$) was comparable to that of the reported excellent enzyme mimic CHF-1 ($k_{cat}/K_m \approx 2.0 \times 10^4$). PCOF-Fe could be reused for three cycles without losing catalytic activity. Meanwhile, PCOF-Co exhibited good electrocatalytic activity towards oxygen evolution reactions. According to the linear sweep voltammograms (LSVs) of PCOF-Co, overpotentials of 473 mV for PCOF-1-Co and 487 mV for PCOF-2-Co were required to achieve a current density of 10 mA cm^{-2}, comparable to that of the cobalt porphyrin-based conjugated mesoporous polymer CoP-4ph-CMP-800. The values of the Tafel slope were estimated to be 89 mV dec^{-1} for PCOF-1-Co and 95 mV dec^{-1} for PCOF-2-Co, comparable to and even lower than those of many other reported catalysts such as CoP-2ph-CMP-800, Ni_3S_2/Ni foam and $CsCo_9$/carbon composites. From the Nyquist plot of PCOF-Co, PCOF-1-Co and PCOF-2-Co have similar charge transfer resistance (R_{ct}). Furthermore, the long-term chronopotential curve showed no significant changes in potential over 50 hours at a catalytic current density of 10 mA cm^{-2}, suggesting good catalytic stability for PCOF-Co.

Other than the skeletons, guests incorporated in the frameworks can also act as the active sites. Heteropolyacids (HPAs) are a classical type of multifunctional catalytic materials, and their immobilization is widely studied all over the world. In the paper posted by Jia and co-workers in 2015, a series of phosphomolybdic acid functionalized 3D COFs (PMA@COF-300a, PMA@COF-300b and PMA@COF-300c) with different preparation conditions and doping levels were reported to catalyze the epoxidation of olefins with *t*-BuOOH as the oxidant.[82] All three PMA@COF-300 composites are active and selective, although their catalytic activities are lower than that of the homogeneous PMA. The catalytic activity of PMA@COF-300b (TOF = 55) is slightly lower than that of the oxodiperoxo molybdenum modified mesoporous materials, but much better than that of PMA functionalized imidazolium-based periodic mesoporous organosilicas. Moreover, PMA@COF-300 catalysts are quite stable under the test conditions and can be used at least three times without significant activity loss.

4.5 Fluorescence

The fast and efficient detection of trace explosives is highly demanded in environmental and security areas. 3D COFs with plenty of channels and fluorophores are promising candidates for explosive detection. In the following work, a pyrene-based, fluorescent 3D COF (3D-Py-COF) was used in explosive detection.[26] Owing to the isolated imine-functionalized pyrene units in the 3D network, 3D-Py-COF showed an intense yellow-green luminescence while no fluorescence was observed for imine-linked 2D Py-COFs. Considering the high porosity and

fluorescence, the chemosensing behavior of 3D-Py-COF was studied. With the gradual addition of model compound picric acid (PA), the fluorescence quenched for 3D-Py-COF and the fluorescence quenching degree reached 75% when the concentration of PA was 20 ppm, indicating sensitivity to PA for 3D-Py-COF. The Stern–Volmer curve quenching constant (K_{SV}) was estimated to be 3.1×10^4 M^{-1}.

Xie and co-workers tested the chemosensing behavior of AIE based 3D COFs (3D-TPE-COF).[28] 3D-TPE-COF can emit yellow light with an emission maximum at 543 nm with a much higher photoluminescence quantum yield (PLQY, 20%) than the powder of the model compound (6.6%), which may be ascribed to the aggregation of TPE units in the 3D framework. PA was chosen as the explosive model again and the fluorescence of 3D-TPE-COF was quenched with gradually increasing PA concentrations, and K_{SV} was estimated to be 3.3×10^4 M^{-1}.

White light-emitting diodes (WLEDs) have attracted extensive attention due to their wide applications in display and lighting systems. Fluorescent 3D COFs can also be used as light-emitting materials. In the same paper, Xie and co-workers reported a prototype WLED by simply coating 3D-TPE-COF onto a commercial blue LED (Fig. 19). Inspired by the yellow fluorescence of 3D-TPE-COF with blue light excitation, the authors explored the possibility of using this 3D COF for WLEDs by homogeneously coating a thin film of 3D-TPE-COF onto the surface of a commercially available blue LED lamp. After that, bright white light was generated when the LED was turned on. The CIE coordinates (0.30 and 0.35) were close to the standard coordinates for pure white light (0.33 and 0.33). Furthermore, the COF-coated WLED was highly stable and can work under continuous driving under ambient conditions for 1200 h, which has seldom been reported for WLEDs with a down-conversion layer of organic compounds.

4.6 Conductivity

3D COFs were evaluated as semiconductors[105] and may exhibit excellent ionic or electric conductivity. In 2017, 3D ionic CD-COF-Li was designed as a potential Li ion solid-state conductor (Fig. 20).[29] Owing to the flexible and dynamic nature of CD, the anionic feature of the network as well as the high capability for entrapping the electrolytes in the confined channels, the ionic conductivity of the material was calculated to be 2.7 mS cm^{-1} at 30 °C, which was among the highest conductivities for all reported crystalline porous materials and conventional polymer electrolytes with/without fillers. The cell can be cycled at a current density of 0.085 mA cm^{-2} for over 220 hours with a relatively stable stripping/plating voltage.

I_2 doping is a common approach for enhancing electrical conductivity in polymers and other porous materials. The first related work was carried out on I_2@COF-DL229 with conductivity up to 1.53×10^{-2} S cm^{-1}, 1990 times greater than the value (7.69×10^{-6} S cm^{-1}) for iodine.[47] Charge transfer between iodine and π-conjugated channel walls of COF-DL229 may account for the sharp increase.

3D-TTF-COFs (JUC-518 and JUC-519) with redox active TTF moieties can be converted to radical cation forms by exposure to I_2 vapor.[27] The conducting properties of 3D-TTF-COFs could be tuned with doping time and temperature. For example, the

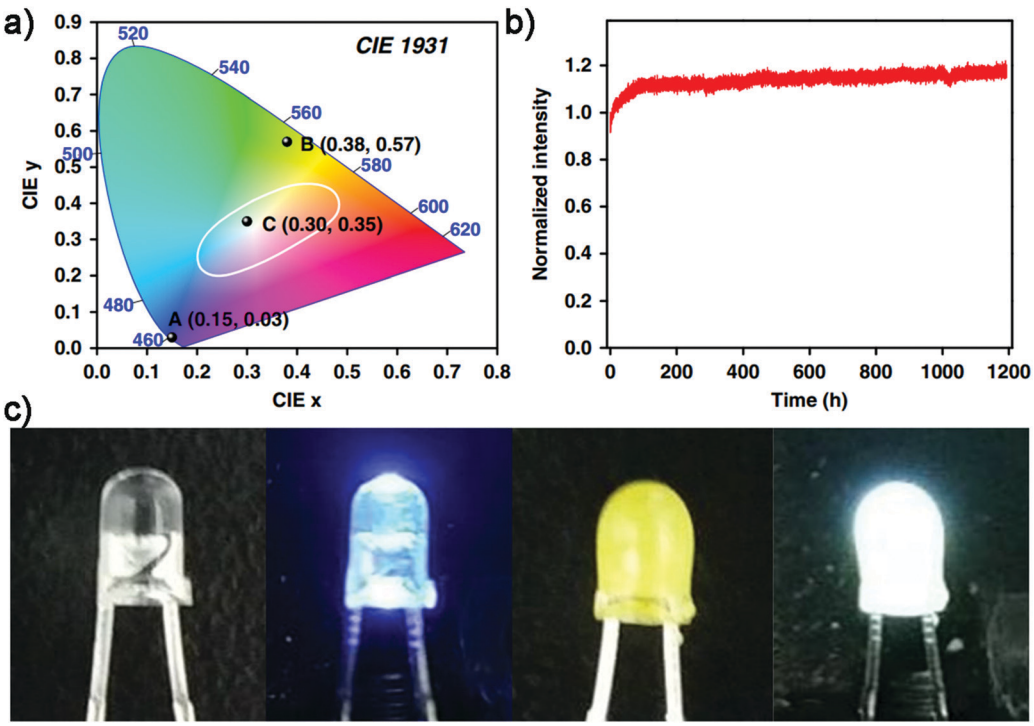

Fig. 19 Characterization and photographs of WLED based on 3D-TPE-COF (reproduced from ref. 28 with permission from Springer Nature, Copyright 2018).

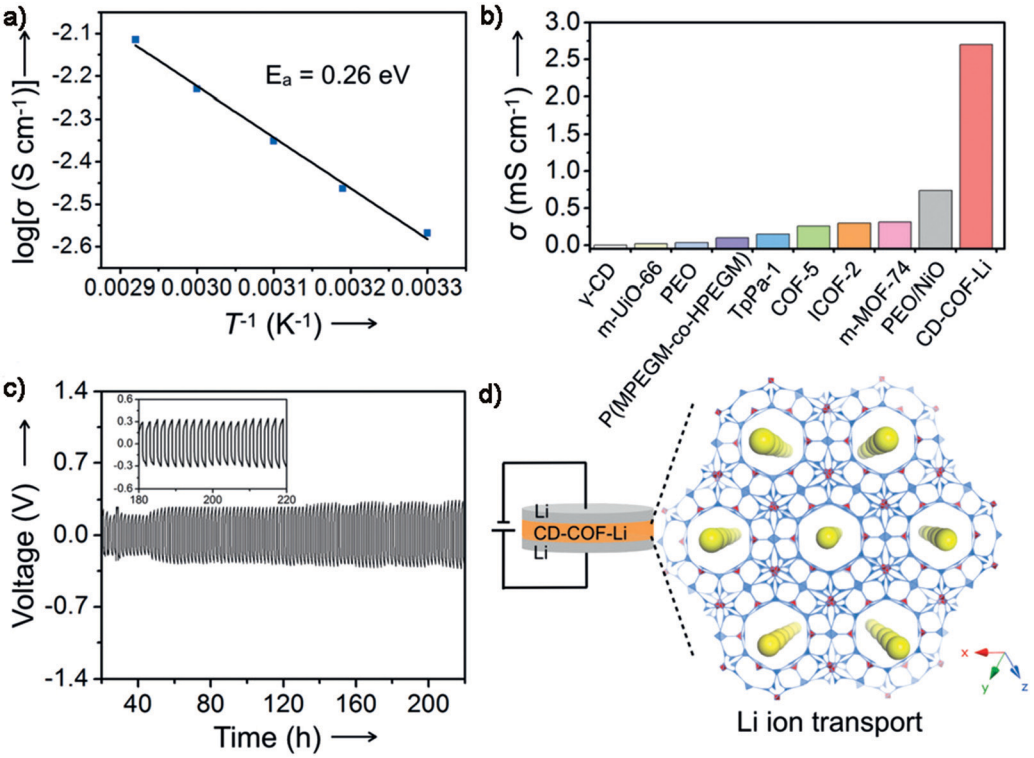

Fig. 20 Li^+ conductivity performance of CD-COF-Li (reproduced from ref. 105 with permission from Wiley-VCH, Copyright 2017).

conductivity was 2.9×10^{-7} S cm^{-1} for JUC-518 at 25 °C after doping for 6 h, and could be increased to 2.7×10^{-4} S cm^{-1} at 25 °C upon doping for 48 h and to 1.4×10^{-2} S cm^{-1} by raising the temperature up to 120 °C. The electrical conductivity of 3D-TTF-COFs is higher than that of 2D TTF-based COFs (about 10^{-5} S cm^{-1}) and comparable to the best performing TTF-based MOFs with the highest conductivity (about 10^{-4} S cm^{-1}). Compared to 2D COFs, interconnected channels and higher surface areas in 3D frameworks may cause more I_2 doping and full oxidation of TTF units as well as the resultant better conducting performance. The stability of I_2 doped 3D-TTF-COFs can be confirmed by repeated test cycles for at least four times without obvious electroactivity loss.

4.7 Solar cell

The research of perovskite solar cells (PSCs) has exploded in the past decade with certified power conversion efficiency (PCE) rocketing from single digit to 22.1%. With uniformly ordered porous frameworks, rigid and long-range conjugated systems (1D conjugated segments) and numerous highly ordered electron-transporting channels in the frameworks, the highly conjugated 3D COFs (SP-3D-COFs) based on the spirobifluorene tetrahedral core were used for PSC enhancement in 2018 (Fig. 21).[49] By simple bulk doping of as-prepared COFs in photovoltaic devices, the average power conversion efficiency was improved by 15.9% for SP-3D-COF 1 and 18.0% for SP-3D-COF 2 as compared to the reference undoped PSC, while excellent leakage prevention was observed in the meantime. Moreover, with the help of density functional theory (DFT) calculations a possible perovskite–SP-3D-COFs interaction mechanism was proposed involving electron transport mobility, absorption, morphology, and so on. These 3D COFs with novel conjugated structures exhibit vast potential for further application as PSC doping materials.

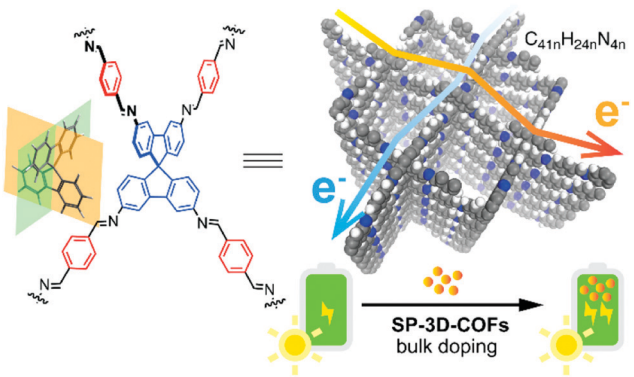

Fig. 21 Schematic representation of SP-3D-COF as PSC doping materials (reproduced from ref. 49 with permission from American Chemical Society, Copyright 2018).

5 Conclusion and perspectives

Since the first successful example reported by Yaghi and co-workers in 2007, 3D COFs have attracted wide interest throughout the world for their unique properties and applications. With highly void frameworks, large surface areas and abundant open

channels, 3D COFs are considered as promising materials for gas uptake, energy storage, *etc.* Moreover, easy modifications can be conducted over 3D COFs as a result of their organic nature. Plenty of different approaches have been developed for the functionalization of 3D COFs and various applications have been exploited including adsorption from solution and heterogeneous catalyses.

However, the achievements in 3D COFs are still insufficient compared to the explosive development of the 2D analogues. There are still some hurdles: (1) the 'crystallization problem' was more serious for 3D structures. Amorphous frameworks were more inclined to be generated for 3D structures because of the absence of additional driving force (mainly π–π stackings). Several other preparation strategies, especially those used in 2D COFs (such as mechanochemical synthesis, flow synthesis or vapour-assisted conversion), MOFs (such as electrochemical synthesis,[106] sonochemical synthesis[107] and high-throughput synthesis[108]) and nanomaterials (nanoscale precipitation,[109] surfactant-templated synthesis,[110] and reverse microemulsion[111]), are still waiting for further exploration in 3D structures. (2) There are only dozens of 3D COFs that have been reported. The introduction of new linkages (such as triazine, azine, hydrazone, urea, alkene, *etc.*) and topologies (such as **tfj**, **fjh**, **iab**, **sod**, **cda**, **cds**, **pcu**, **acs**, **bcu**, **ttt**, *etc.*) might be a possible approach to enrich the library. Furthermore, the development of MOF materials connected by covalent bonds will probably open an avenue to a brand-new kind of 3D frameworks. For example, Yaghi and co-workers reported a new 3D MOF (MOF-688) that was synthesized by linking ditopic amino functionalized polyoxometalate $[N(C_4H_9)_4]_3[MnMo_6O_{18}\{(OCH_2)_3CNH_2\}_2]$ with 4-connected tetrahedral tetrakis(4-formylphenyl)methane building units through imine condensation, in which the polyoxometalate cluster seems like another linkage in 3D COFs.[112] (3) Interpenetration is common in 3D networks with **dia**, **pts** or **srs** topologies, especially in some void structures. Specific surface areas, pore volumes and pore sizes were decreased significantly with increasing interpenetration numbers. Moreover, only 1D uniform channels remain in high interpenetrated backbones while 3D connected channels exist in non-interpenetrated or low interpenetrated frameworks. Some works to control the interpenetration have been conducted in recent years but various factors still need inquiry, including monomers, preparation methods and synthesis conditions. It should be noted that the employment of monomer TAA is a useful strategy for avoiding or decreasing interpenetration, which was used in the first non-interpenetrated **dia** or **pts** COF. (4) The structure identification is still a key problem in 3D COFs, especially for interpenetrated structures or new topologies. Since most COFs are obtained as polycrystalline materials, the general approach nowadays is powder X-ray diffraction in combination with structural simulation. Without the assistance of π–π stackings, much more possible structures have to be considered if the obtained structure is not as expected. The growth of single crystals might be the ultimate solution but is still not mature because of the difficulties in obtaining COF single crystals with sufficient sizes. 3D electron diffraction using the RED method was also used for resolution of some small single crystals. (5) The applications are still limited in 3D COFs. Mild functionalization approaches were required in 3D COFs since most 3D COFs demonstrated lower stability than 2D structures due to the absence of π–π stacking. Post-modification was often conducted in combination with bottom-up or *in situ* approaches. Some strategies employed in 2D COFs or other porous materials might have borrowed meanings.

In summary, we have discussed the design principles (topologies and linkages, building blocks), synthetic methods and functionalized strategies (bottom-up, *in situ* and post-modification) of 3D COFs. The potential applications of functional 3D COFs are highlighted including adsorption and separation, heterogeneous catalysis, fluorescence, conductivity, solar cells, *etc.* We believe that this review can provide potential guidance for the synthesis of functional 3D COFs in the near future.

Abbreviations

$[BMIm][N(CN)_2]$	1-Butyl-3-methylimidazolium dicyanamide
$[BMIm][NTf_2]$	1-Butyl-3-methylimidazolium bis((trifluoromethyl)sulfonyl)imide
$[Emim][Tf_2N]$	1-Ethyl-3-methylimidazolium bis(trifluoromethylsulfonyl)imide
1D	One dimensional
2D	Two dimensional
3D	Three dimensional
ABTS	2,2′-Azinodi(3-ethylbenzothiazoline)-6-sulfonate
AIE	Aggregation-induced emission
ANG	Adsorbed natural gas
APTES	3-Aminopropyltriethoxysilane
BFBZ	4,7-Bis(4-formylbenzyl)-1*H*-benzimidazole
BPDA	Biphenyl-4,4′-dicarbaldehyde
BpyDA	(3,3′-Bipyridine)-6,6′-dicarbaldehyde
C-THBA	4′,4‴,4⁗,4⁗′-Methanetetrayltetrakis(4′-hydroxy-1,1′-biphenyl-3′-carbaldehyde)
COF	Covalent organic framework
CD	Cyclodextrin
CHDA	*trans*-1,4-Cyclohexyldiamine
DABP	4,4′-Diaminobiphenyl
DATP	4,4″-Diamino-*p*-terphenyl
DB	Dimidium bromide
DBA	Dehydrobenzoannulene
DCPDA	4,5-Dichlorophenylene-1,2-diamine
DFPDA	4,5-Difluorophenylene-1,2-diamine
DFT	Density functional theory
DHBD	3,3′-Dihydroxybenzidine
DHTA	2,5-Dihydroxyterephthalaldehyde
DIP	Diiminopyridine
DMA	9,10-Dimethylanthracene
DOE	Department of Energy
DSC	Differential scanning calorimetry
EB	Ethidium bromide

ETTA	4,4″,4″,4‴-(Ethene-1,1,2,2-tetrayl)tetraaniline
FE	Faradaic efficiency
FF	Force fields
FFPBA	2-Fluoro-4-formylphenylboronic acid
FPBA	4-Formylphenylboronic acid
FTIR	Fourier transform infrared spectroscopy
GCMC	Grand canonical Monte Carlo
HHTP	2,3,6,7,10,11-Hexahydroxytriphenylene
HN	Hydroxynaphthol blue disodium salt
HOPG	Highly ordered pyrolytic graphite
HPA	Heteropolyacids
HPLC	High performance liquid chromatography
IBU	Ibuprofen
LSVs	Linear sweep voltammograms
MMM	Mixed matrix membranes
MB	Methyl blue
MO	Methyl orange
MOF	Metal organic framework
MTABC	4,4′,4″,4‴-Methanetetraaryltetrabenzoyl chloride
MTMS	Methyltrimethoxysilane
NMR	Nuclear magnetic resonance
PA	Picric acid
PANI	Polyaniline
PCBA	2,6-Pyridinedicarboxaldehyde
PDA	1,4-Phenylenediamine
PDB	4,4′-(1,10-Phenanthroline-2,9-diyl)dibenzaldehyde
PEI	Poly(ethyleneimine)
PLQY	Photoluminescence quantum yield
PMA	Phosphomolybdic acid
PMDA	Pyromellitic dianhydride
PSCs	Perovskite solar cells
PXRD	Powder X-ray diffraction
R_{ct}	Charge transfer resistance
QM	Quantum mechanics
RED	Rotation electron diffraction
RH	Relative humidity
Si-THBA	4′,4‴,4⁗,4⁗′-Silanetetrayltetrakis-(4-hydroxy-[1,1′-biphenyl]-3-carbaldehyde)
SA	Succinic anhydride
SEM	Scanning electron microscope
SLG	Single-layered graphite
SP	Spirobifluorene
SXRD	Single-crystal X-ray diffraction
TA	Terephthaldehyde
TAA	1,3,5,7-Tetraaminoadamantane
TABPE	1,1,2,2-Tetrakis(4-amino-(1,1′-biphenyl))ethene
TADDOL	Tetraaryl-1,3-dioxolane-4,5-dimethanols
TANM	Tetra(*p*-amino naphthyl)methane
TAPA	1,3,5,7-Tetrakis(4-aminophenyl)adamantine
TAPB	1,3,5-Tris(4-aminophenyl)benzene
TAPM	Tetrakis(4-aminophenyl)methane
TAPP	5,10,15,20-Tetrakis(4-aminophenyl)-porphyrin
TABPP	5,10,15,20-Tetrakis(4-amino-(1,1′-biphenyl))porphyrin
TASP	(3,3′,6,6′-Tetraamine-9,9′-spirobifluorene)
TbPM	Tetra(1,1′-biphenyl-4-yl)methane
TbPS	Tetra(1,1′-biphenyl-4-yl)silane
TBPM	Tetra(4-dihydroxyborylphenyl)methane
TBPS	Tetra(4-dihydroxyborylphenyl)silane
TFB	1,3,5-Triformylbenzene
TFBM	3,3′,5,5′-Tetrakis(4-formylphenyl)bimesityl
TFBPE	1,1,2,2-Tetrakis(4-formyl-(1,1′-biphenyl))ethene
TFHPM	Tetrakis(3-formyl-4-hydroxylphenyl)methane
TFP	Triformylphloroglucinol
TFPA	Tris(4-formylphenyl)amine
TFPB	1,3,5-Tris(4-formylphenyl)benzene
TFPM	Tetrakis(4-formylphenyl)methane
TFPP	5,10,15,20-Tetrakis(4-formylphenyl)porphyrin
TFPPy	1,3,6,8-Tetrakis(4-formylphenyl) pyrene
TFPS	Tetrakis(4-formylphenyl)silane
TGA	Thermogravimetric analysis
TML	Truncated mixed-linker
TNPM	Tetrakis(4-nitrosophenyl)methane
TNPS	Tetrakis(4-nitrosophenyl)silane
TNPA	1,3,5,7-Tetrakis(4-nitrosophenyl)-adamantane
TPA	Tetraphenyladamantine
TPB	1,2,4,5-Tetraphenylbenzene
TPM	Tetraphenylmethane
TPS	Tetraphenylsilane
TTF-TBA	Tetrathiafulvalene-tetrabenzaldehyde
WLEDs	White light-emitting diode

Conflicts of interest

There are no conflicts to declare.

Acknowledgements

This work was supported by the National Natural Science Foundation of China (21571079, 21621001, 21390394, 21571076, and 21571078), ''111'' project (B07016 and B17020), and the program for JLU Science and Technology Innovative Research Team. Q. F. acknowledges the Thousand Talents program (China).

Notes and references

1 A. P. Cote, A. I. Benin, N. W. Ockwig, M. O'Keeffe, A. J. Matzger and O. M. Yaghi, *Science*, 2005, **310**, 1166–1170.
2 H. Furukawa and O. M. Yaghi, *J. Am. Chem. Soc.*, 2009, **131**, 8875–8883.
3 E. Tylianakis, E. Klontzas and G. E. Froudakis, *Nanoscale*, 2011, **3**, 856–869.
4 M. O'Keeffe, *Chem. Soc. Rev.*, 2009, **38**, 1215–1217.

5 H. C. Zhou, J. R. Long and O. M. Yaghi, *Chem. Rev.*, 2012, **112**, 673–674.
6 M. S. Lohse, T. Stassin, G. Naudin, S. Wuttke, R. Ameloot, D. De Vos, D. D. Medina and T. Bein, *Chem. Mater.*, 2016, **28**, 626–631.
7 X. Guan, H. Li, Y. Ma, M. Xue, Q. Fang, Y. Yan, V. Valtchev and S. Qiu, *Nat. Chem.*, 2019, **11**, 587–594.
8 S. Y. Ding, J. Gao, Q. Wang, Y. Zhang, W. G. Song, C. Y. Su and W. Wang, *J. Am. Chem. Soc.*, 2011, **133**, 19816–19822.
9 U. Díaz and A. Corma, *Coord. Chem. Rev.*, 2016, **311**, 85–124.
10 X. Ding, J. Guo, X. Feng, Y. Honsho, J. Guo, S. Seki, P. Maitarad, A. Saeki, S. Nagase and D. Jiang, *Angew. Chem., Int. Ed.*, 2011, **50**, 1289–1293.
11 L. Yang and D.-C. Wei, *Chin. Chem. Lett.*, 2016, **27**, 1395–1404.
12 L. Ma, S. Wang, X. Feng and B. Wang, *Chin. Chem. Lett.*, 2016, **27**, 1383–1394.
13 M. Dogru and T. Bein, *Chem. Commun.*, 2014, **50**, 5531–5546.
14 H. V. Babu, M. G. M. Bai and M. Rajeswara Rao, *ACS Appl. Mater. Interfaces*, 2019, **11**, 11029–11060.
15 S. Dalapati, S. Jin, J. Gao, Y. Xu, A. Nagai and D. Jiang, *J. Am. Chem. Soc.*, 2013, **135**, 17310–17313.
16 N. Huang, P. Wang and D. Jiang, *Nat. Rev. Mater.*, 2016, **1**, 0056.
17 Y. Song, Q. Sun, B. Aguila and S. Ma, *Adv. Sci.*, 2019, **6**, 1801410.
18 P. J. Waller, F. Gandara and O. M. Yaghi, *Acc. Chem. Res.*, 2015, **48**, 3053–3063.
19 S. Kandambeth, K. Dey and R. Banerjee, *J. Am. Chem. Soc.*, 2019, **141**, 1807–1822.
20 R. Zhu, J. Ding, L. Jin and H. Pang, *Coord. Chem. Rev.*, 2019, **389**, 119–140.
21 X. Ma and T. F. Scott, *Commun. Chem.*, 2018, **1**, 98.
22 H. M. El-Kaderi, J. R. Hunt, J. L. Mendoza-Cortes, A. P. Cote, R. E. Taylor, M. O'Keeffe and O. M. Yaghi, *Science*, 2007, **316**, 268–272.
23 R. Babarao, R. Custelcean, B. P. Hay and D.-E. Jiang, *Cryst. Growth Des.*, 2012, **12**, 5349–5356.
24 F. J. Uribe-Romo, J. R. Hunt, H. Furukawa, C. Klock, M. O'Keeffe and O. M. Yaghi, *J. Am. Chem. Soc.*, 2009, **131**, 4570–4571.
25 Q. Fang, J. Wang, S. Gu, R. B. Kaspar, Z. Zhuang, J. Zheng, H. Guo, S. Qiu and Y. Yan, *J. Am. Chem. Soc.*, 2015, **137**, 8352–8355.
26 G. Lin, H. Ding, D. Yuan, B. Wang and C. Wang, *J. Am. Chem. Soc.*, 2016, **138**, 3302–3305.
27 H. Li, J. Chang, S. Li, X. Guan, D. Li, C. Li, L. Tang, M. Xue, Y. Yan, V. Valtchev, S. Qiu and Q. Fang, *J. Am. Chem. Soc.*, 2019, **141**, 13324–13329.
28 H. Ding, J. Li, G. Xie, G. Lin, R. Chen, Z. Peng, C. Yang, B. Wang, J. Sun and C. Wang, *Nat. Commun.*, 2018, **9**, 5234.
29 Y. Zhang, J. Duan, D. Ma, P. Li, S. Li, H. Li, J. Zhou, X. Ma, X. Feng and B. Wang, *Angew. Chem., Int. Ed.*, 2017, **56**, 16313–16317.
30 O. Yahiaoui, A. N. Fitch, F. Hoffmann, M. Froba, A. Thomas and J. Roeser, *J. Am. Chem. Soc.*, 2018, **140**, 5330–5333.
31 Y. Lan, X. Han, M. Tong, H. Huang, Q. Yang, D. Liu, X. Zhao and C. Zhong, *Nat. Commun.*, 2018, **9**, 5274.
32 S. Bureekaew and R. Schmid, *CrystEngComm*, 2013, **15**, 1551–1562.
33 N. C. Duncan, B. P. Hay, E. W. Hagaman and R. Custelcean, *Tetrahedron*, 2012, **68**, 53–64.
34 C. S. Diercks and O. M. Yaghi, *Science*, 2017, **355**, eaal1585.
35 P. Kuhn, M. Antonietti and A. Thomas, *Angew. Chem., Int. Ed.*, 2008, **47**, 3450–3453.
36 D. N. Bunck and W. R. Dichtel, *J. Am. Chem. Soc.*, 2013, **135**, 14952–14955.
37 C. Zhao, C. S. Diercks, C. Zhu, N. Hanikel, X. Pei and O. M. Yaghi, *J. Am. Chem. Soc.*, 2018, **140**, 16438–16441.
38 E. Jin, M. Asada, Q. Xu, S. Dalapati, M. A. Addicoat, M. A. Brady, H. Xu, T. Nakamura, T. Heine, Q. Chen and D. Jiang, *Science*, 2017, **357**, 673–676.
39 J. L. Segura, M. J. Mancheno and F. Zamora, *Chem. Soc. Rev.*, 2016, **45**, 5635–5671.
40 Q. Fang, S. Gu, J. Zheng, Z. Zhuang, S. Qiu and Y. Yan, *Angew. Chem., Int. Ed.*, 2014, **53**, 2878–2882.
41 J. R. Hunt, C. J. Doonan, J. D. LeVangie, A. P. Cote and O. M. Yaghi, *J. Am. Chem. Soc.*, 2008, **130**, 11872–11873.
42 D. Beaudoin, T. Maris and J. D. Wuest, *Nat. Chem.*, 2013, **5**, 830–834.
43 D. Stewart, D. Antypov, M. S. Dyer, M. J. Pitcher, A. P. Katsoulidis, P. A. Chater, F. Blanc and M. J. Rosseinsky, *Nat. Commun.*, 2017, **8**, 1102.
44 Z. Li, H. Li, X. Guan, J. Tang, Y. Yusran, Z. Li, M. Xue, Q. Fang, Y. Yan, V. Valtchev and S. Qiu, *J. Am. Chem. Soc.*, 2017, **139**, 17771–17774.
45 S. Yan, X. Guan, H. Li, D. Li, M. Xue, Y. Yan, V. Valtchev, S. Qiu and Q. Fang, *J. Am. Chem. Soc.*, 2019, **141**, 2920–2924.
46 T. Ma, E. A. Kapustin, S. X. Yin, L. Liang, Z. Zhou, J. Niu, L. H. Li, Y. Wang, J. Su, J. Li, X. Wang, W. D. Wang, W. Wang, J. Sun and O. M. Yaghi, *Science*, 2018, **361**, 48–52.
47 C. Wang, Y. Wang, R. Ge, X. Song, X. Xing, Q. Jiang, H. Lu, C. Hao, X. Guo, Y. Gao and D. Jiang, *Chem. – Eur. J.*, 2018, **24**, 585–589.
48 J. Huang, X. Han, S. Yang, Y. Cao, C. Yuan, Y. Liu, J. Wang and Y. Cui, *J. Am. Chem. Soc.*, 2019, **141**, 8996–9003.
49 C. Wu, Y. Liu, H. Liu, C. Duan, Q. Pan, J. Zhu, F. Hu, X. Ma, T. Jiu, Z. Li and Y. Zhao, *J. Am. Chem. Soc.*, 2018, **140**, 10016–10024.
50 X. Han, J. Huang, C. Yuan, Y. Liu and Y. Cui, *J. Am. Chem. Soc.*, 2018, **140**, 892–895.
51 Y. Liu, Y. Ma, Y. Zhao, X. Sun, F. Gandara, H. Furukawa, Z. Liu, H. Zhu, C. Zhu, K. Suenaga, P. Oleynikov, A. S. Alshammari, X. Zhang, O. Terasaki and O. M. Yaghi, *Science*, 2016, **351**, 365–369.
52 Y. Liu, C. S. Diercks, Y. Ma, H. Lyu, C. Zhu, S. A. Alshmimri, S. Alshihri and O. M. Yaghi, *J. Am. Chem. Soc.*, 2019, **141**, 677–683.
53 Y. Zhao, L. Guo, F. Gandara, Y. Ma, Z. Liu, C. Zhu, H. Lyu, C. A. Trickett, E. A. Kapustin, O. Terasaki and O. M. Yaghi, *J. Am. Chem. Soc.*, 2017, **139**, 13166–13172.

54 N. L. Campbell, R. Clowes, L. K. Ritchie and A. I. Cooper, *Chem. Mater.*, 2009, **21**, 204–206.
55 X. Guan, Y. Ma, H. Li, Y. Yusran, M. Xue, Q. Fang, Y. Yan, V. Valtchev and S. Qiu, *J. Am. Chem. Soc.*, 2018, **140**, 4494–4498.
56 C. Qian, Q. Y. Qi, G. F. Jiang, F. Z. Cui, Y. Tian and X. Zhao, *J. Am. Chem. Soc.*, 2017, **139**, 6736–6743.
57 Z. Li, X. Ding, Y. Feng, W. Feng and B.-H. Han, *Macromolecules*, 2019, **52**, 1257–1265.
58 D. Wu, F. Xu, B. Sun, R. Fu, H. He and K. Matyjaszewski, *Chem. Rev.*, 2012, **112**, 3959–4015.
59 B. P. Biswal, S. Chandra, S. Kandambeth, B. Lukose, T. Heine and R. Banerjee, *J. Am. Chem. Soc.*, 2013, **135**, 5328–5331.
60 Y. Peng, W. K. Wong, Z. Hu, Y. Cheng, D. Yuan, S. A. Khan and D. Zhao, *Chem. Mater.*, 2016, **28**, 5095–5101.
61 Y. Jiang, W. Huang, J. Wang, Q. Wu, H. Wang, L. Pan and X. Liu, *J. Mater. Chem. A*, 2014, **2**, 8201–8204.
62 Y. B. Zhang, J. Su, H. Furukawa, Y. Yun, F. Gandara, A. Duong, X. Zou and O. M. Yaghi, *J. Am. Chem. Soc.*, 2013, **135**, 16336–16339.
63 A. M. Evans, L. R. Parent, N. C. Flanders, R. P. Bisbey, E. Vitaku, M. S. Kirschner, R. D. Schaller, L. X. Chen, N. C. Gianneschi and W. R. Dichtel, *Science*, 2018, **361**, 52–57.
64 H. Wang, Z. Zeng, P. Xu, L. Li, G. Zeng, R. Xiao, Z. Tang, D. Huang, L. Tang, C. Lai, D. Jiang, Y. Liu, H. Yi, L. Qin, S. Ye, X. Ren and W. Tang, *Chem. Soc. Rev.*, 2019, **48**, 488–516.
65 R. P. Bisbey, C. R. DeBlase, B. J. Smith and W. R. Dichtel, *J. Am. Chem. Soc.*, 2016, **138**, 11433–11436.
66 D. D. Medina, J. M. Rotter, Y. Hu, M. Dogru, V. Werner, F. Auras, J. T. Markiewicz, P. Knochel and T. Bein, *J. Am. Chem. Soc.*, 2015, **137**, 1016–1019.
67 K. Dey, M. Pal, K. C. Rout, H. S. Kunjattu, A. Das, R. Mukherjee, U. K. Kharul and R. Banerjee, *J. Am. Chem. Soc.*, 2017, **139**, 13083–13091.
68 M. Matsumoto, L. Valentino, G. M. Stiehl, H. B. Balch, A. R. Corcos, F. Wang, D. C. Ralph, B. J. Mariñas and W. R. Dichtel, *Chem*, 2018, **4**, 308–317.
69 H. Lu, C. Wang, J. Chen, R. Ge, W. Leng, B. Dong, J. Huang and Y. Gao, *Chem. Commun.*, 2015, **51**, 15562–15565.
70 J. Fu, S. Das, G. Xing, T. Ben, V. Valtchev and S. Qiu, *J. Am. Chem. Soc.*, 2016, **138**, 7673–7680.
71 Y. Cheng, L. Zhai, Y. Ying, Y. Wang, G. Liu, J. Dong, D. Z. L. Ng, S. A. Khan and D. Zhao, *J. Mater. Chem. A*, 2019, **7**, 4549–4560.
72 H. Li, Q. Pan, Y. Ma, X. Guan, M. Xue, Q. Fang, Y. Yan, V. Valtchev and S. Qiu, *J. Am. Chem. Soc.*, 2016, **138**, 14783–14788.
73 D. N. Bunck and W. R. Dichtel, *Angew. Chem., Int. Ed.*, 2012, **51**, 1885–1889.
74 S. D. Brucks, D. N. Bunck and W. R. Dichtel, *Polymer*, 2014, **55**, 330–334.
75 G. Lin, H. Ding, R. Chen, Z. Peng, B. Wang and C. Wang, *J. Am. Chem. Soc.*, 2017, **139**, 8705–8709.
76 C. Wang, Y. Meng, Y. Luo, J. L. Shi, H. Ding, X. Lang, W. Chen, A. Zheng and J. Sun, *Angew. Chem., Int. Ed.*, 2019, DOI: 10.1002/anie.201913091.
77 D. N. Bunck and W. R. Dichtel, *Chem. Commun.*, 2013, **49**, 2457–2459.
78 Q. Lu, Y. Ma, H. Li, X. Guan, Y. Yusran, M. Xue, Q. Fang, Y. Yan, S. Qiu and V. Valtchev, *Angew. Chem., Int. Ed.*, 2018, **57**, 6042–6048.
79 H. Liu, J. Chu, Z. Yin, X. Cai, L. Zhuang and H. Deng, *Chem*, 2018, **4**, 1696–1709.
80 L. A. Baldwin, J. W. Crowe, D. A. Pyles and P. L. McGrier, *J. Am. Chem. Soc.*, 2016, **138**, 15134–15137.
81 Y. Liu, X. Yan, T. Li, W.-D. Zhang, Q.-T. Fu, H.-S. Lu, X. Wang and Z.-G. Gu, *New J. Chem.*, 2019, **43**, 16907–16914.
82 W. Gao, X. Sun, H. Niu, X. Song, K. Li, H. Gao, W. Zhang, J. Yu and M. Jia, *Microporous Mesoporous Mater.*, 2015, **213**, 59–67.
83 Y. Xin, C. Wang, Y. Wang, J. Sun and Y. Gao, *RSC Adv.*, 2017, **7**, 1697–1700.
84 S. S. Han, H. Furukawa, O. M. Yaghi and W. A. Goddard, 3rd, *J. Am. Chem. Soc.*, 2008, **130**, 11580–11581.
85 B. Assfour and G. Seifert, *Microporous Mesoporous Mater.*, 2010, **133**, 59–65.
86 A. R. V. Koenig, C. Desgranges and J. Delhommelle, *Mol. Simul.*, 2013, **40**, 71–79.
87 B. Assfour and G. Seifert, *Chem. Phys. Lett.*, 2010, **489**, 86–91.
88 P. Srepusharawoot, R. H. Scheicher, C. Moysés Araújo, A. Blomqvist, U. Pinsook and R. Ahuja, *J. Phys. Chem. C*, 2009, **113**, 8498–8504.
89 E. Klontzas, E. Tylianakis and G. E. Froudakis, *Nano Lett.*, 2010, **10**, 452–454.
90 D. Cao, J. Lan, W. Wang and B. Smit, *Angew. Chem., Int. Ed.*, 2009, **48**, 4730–4733.
91 E. Klontzas, E. Tylianakis and G. E. Froudakis, *J. Phys. Chem. C*, 2009, **113**, 21253–21257.
92 J. Lan, D. Cao and W. Wang, *J. Phys. Chem. C*, 2010, **114**, 3108–3114.
93 T.-F. Gao and H. Zhang, *Struct. Chem.*, 2013, **25**, 503–513.
94 Z. Ke, Y. Cheng, S. Yang, F. Li and L. Ding, *Int. J. Hydrogen Energy*, 2017, **42**, 11461–11468.
95 F. Li, J. J. Zhao, B. Johansson and L. X. Sun, *Int. J. Hydrogen Energy*, 2010, **35**, 266–271.
96 X. Zou, G. Zhou, W. Duan, K. Choi and J. Ihm, *J. Phys. Chem. C*, 2010, **114**, 13402–13407.
97 J. L. Mendoza-Cortes, S. S. Han, H. Furukawa, O. M. Yaghi and W. A. Goddard 3rd, *J. Phys. Chem. A*, 2010, **114**, 10824–10833.
98 J. Lan, D. Cao and W. Wang, *Langmuir*, 2010, **26**, 220–226.
99 J. L. Mendoza-Cortes, T. A. Pascal and W. A. Goddard 3rd, *J. Phys. Chem. A*, 2011, **115**, 13852–13857.
100 R. Mercado, R.-S. Fu, A. V. Yakutovich, L. Talirz, M. Haranczyk and B. Smit, *Chem. Mater.*, 2018, **30**, 5069–5086.
101 Y. X. Ma, Z. J. Li, L. Wei, S. Y. Ding, Y. B. Zhang and W. Wang, *J. Am. Chem. Soc.*, 2017, **139**, 4995–4998.
102 Y. Lan, M. Tong, Q. Yang and C. Zhong, *CrystEngComm*, 2017, **19**, 4920–4926.

103 C. Gao, J. Li, S. Yin, G. Lin, T. Ma, Y. Meng, J. Sun and C. Wang, *Angew. Chem., Int. Ed.*, 2019, **58**, 9770–9775.
104 Y. Liu, Y. Ma, J. Yang, C. S. Diercks, N. Tamura, F. Jin and O. M. Yaghi, *J. Am. Chem. Soc.*, 2018, **140**, 16015–16019.
105 B. Lukose, A. Kuc and T. Heine, *J. Mol. Model.*, 2013, **19**, 2143–2148.
106 U. Mueller, H. Puetter, M. Hesse and H. Wessel, WO 2005/049892, 2005.
107 L. G. Qiu, Z. Q. Li, Y. Wu, W. Wang, T. Xu and S. Jiang, *Chem. Commun.*, 2008, 3642–3644.
108 R. Banerjee, A. Phan, B. Wang, C. Knobler, H. Furukawa, M. O'Keeffe and O. M. Yaghi, *Science*, 2008, **319**, 939–943.
109 W. J. Rieter, K. M. Pott, K. M. L. Taylor and W. Lin, *J. Am. Chem. Soc.*, 2008, **130**, 11584–11585.
110 K. M. Taylor, A. Jin and W. Lin, *Angew. Chem., Int. Ed.*, 2008, **47**, 7722–7725.
111 W. J. Rieter, K. M. Taylor, H. An and W. Lin, *J. Am. Chem. Soc.*, 2006, **128**, 9024–9025.
112 W. T. Xu, X. K. Pei, C. S. Diercks, H. Lyu, Z. Ji and O. M. Yaghi, *J. Am. Chem. Soc.*, 2019, **44**, 17522–17526.